Nanoscale

ROYAL SOCIETY OF CHEMISTRY

REVIEW

View Article Online
View Journal | View Issue

Check for updates

Cite this: *Nanoscale*, 2025, **17**, 9619

# MXenes in microbiology and virology: from pathogen detection to antimicrobial applications

Begüm Sarac, [a] Seydanur Yücer [a] and Fatih Ciftci *[a,b]

MXenes, a rapidly emerging class of two-dimensional materials, have demonstrated exceptional versatility and functionality across various domains, including microbiology and virology. Recent advancements in MXene synthesis techniques, encompassing both top-down and bottom-up approaches, have expanded their potential applications in pathogen detection, antimicrobial treatments, and biomedical platforms. This review highlights the unique physicochemical properties of MXenes, including their large surface area, tunable surface chemistry, and high biocompatibility, which contribute to their antimicrobial efficacy against bacteria, fungi, and viruses, such as SARS-CoV-2. The antibacterial mechanisms of MXenes, including membrane disruption, reactive oxygen species (ROS) generation, and photothermal inactivation, are discussed alongside hybridization strategies that enhance their bioactivity. Additionally, the challenges and future prospects of MXenes in developing advanced antimicrobial coatings, diagnostic tools, and therapeutic systems are outlined. By addressing current limitations and exploring innovative solutions, this study underscores the transformative potential of MXenes in microbiology, virology, and biomedical applications.

Received 1st February 2025,
Accepted 24th February 2025

DOI: 10.1039/d5nr00477b

rsc.li/nanoscale

Published on 26 1446. Downloaded on 13/11/47 04:29:14 .

## 1. Introduction

MXenes are a distinctive group of two-dimensional transition metal carbides, nitrides, and carbide-nitrides that have garnered significant attention due to their exceptional physicochemical characteristics and multifunctionality.[1] Their unique structural features, such as a high specific surface area, versatile surface chemistry, and excellent electrical conductivity, make them strong candidates for a wide range of applications. Discovered in 2011, MXenes comprise around 30 different members, each with unique chemical compositions and structures, with new variants being regularly identified. The ease of their synthesis and stability in both water and various organic solvents in the form of colloidal suspensions make MXenes relatively easy to process and scale up. Their antimicrobial properties and versatility are especially valuable for microbiology and virology. Furthermore, the combination of hydrophilicity and high conductivity positions MXenes as promising materials for applications in energy storage, electromagnetic interference shielding, and transparent conductive electrodes. Since their discovery, MXenes have proven to outperform many other existing 2D materials across a variety of fields.[2,3] The synthesis of MXenes has been a critical factor in their development, with advancements in top-down and bottom-up approaches expanding their applicability. Top-down methods, such as selective chemical etching, have evolved to include safer etchants like LiF/HCl and $NH_4HF_2$, reducing toxicity and improving biocompatibility. Bottom-up methods, including chemical vapor deposition and salt-templated synthesis, offer precise control over MXene structure and properties, although challenges remain in scalability and biocompatibility. These synthesis advancements have enabled MXenes to be tailored for applications in antimicrobial coatings, biosensors, and therapeutic platforms.[4] Recent studies have highlighted the antimicrobial mechanisms of MXenes, which include bacterial membrane disruption *via* sharp nanoflake edges, ROS generation, and photothermal inactivation. Hybridization with other organic and inorganic materials has further enhanced their biocidal activity, broadening their use in biomedical devices, water purification systems, and disinfection technologies. The antiviral potential of MXenes, particularly against viruses such as SARS-CoV-2, underscores their relevance during global health crises.[5] This review explores the recent progress in MXene synthesis and their applications in pathogen detection and antimicrobial platforms.[6] Furthermore, the challenges and future opportunities in developing MXene-based technologies for clinical and environmental applications are discussed, providing a comprehensive perspective on their potential impact on microbiology and virology.[4,7]

[a]*Faculty of Engineering, Department of Biomedical Engineering, Fatih Sultan Mehmet Vakif University, Istanbul, Turkey. E-mail: faciftcii@gmail.com*
[b]*Department of Technology Transfer Office, Fatih Sultan Mehmet Vakif University, Istanbul, Turkey*

Published on 26 1446. Downloaded on 13/11/47 04:29:14 .

## 2. Recent advances in MXene synthesis techniques

The advancement of synthesis methods for MXenes has greatly influenced their electrical and physicochemical properties, as well as their diverse applications. Broadly, MXene synthesis can be categorized into three main approaches: etching, top-down techniques, and bottom-up methods.

### 2.1. Etching method

MXenes can be synthesized using several different methods. Innovative etching techniques have made it possible to introduce various terminal groups to the M atoms, aiding in the completion of their coordination environments and lowering surface Gibbs free energy. As a result, the surface characteristics of MXenes play a crucial role in their synthesis process. The subsequent discussion will explore the different preparation methods available.

**2.1.1. Etching with hydrofluoric acid (HF).** The HF acid etching method is one of the most commonly employed techniques for synthesizing MXene materials. This approach has been widely used to produce $Ti_3AlC_2$ from the MAX phase. During the HF acid etching process, Al layers are selectively removed from $Ti_3AlC_2$ and replaced by hydrogen. When $Ti_3C_2$ reacts with deionized water, it forms $Ti_3C_2T_x$ (where T represents surface terminations such as –O, –F, and –OH) along with the release of $H_2$ gas. Additionally, HF acid etching has been successfully applied to convert various MAX phases, including $Ti_2AlC$, $(Ti_{0.5}Nb_{0.5})_2AlC$, $Ti_3AlCN$, $Ta_4AlC_3$, $(V_{0.5}Cr_{0.5})_3AlC_2$, $Nb_2AlC$, $Zr_3Al_3C_5$, $Ti_3SiC_2$, and $Mo_2Ga_2C$, into MXenes. This method remains one of the most effective approaches for MXene synthesis due to its versatility. Extensive research has been conducted to optimize key parameters, such as reaction time, temperature, and fluoride ion concentration, which are critical for achieving high-quality MXene layers. The HF etching process introduces –O, –OH, and –F functional groups to the MXene surface while maintaining the material's intrinsic surface characteristics. Recent investigations have provided detailed insights into the atomic-scale etching behavior of $Ti_3AlC_2$, enhancing the understanding of this process.[8]

**2.1.2. Modified acid etching approach.** Acid fluoride solutions are known for their corrosive and toxic nature. As a result, alternative methods are being developed to replace the direct use of HF acid for removing aluminum layers from MAX phases. One such approach substitutes pure HF acid with a combination of fluoride salts and HCl. However, this method often leads to the formation of a by-product, $AlF_3{\cdot}3H_2O$, during the etching of Al or Ga layers in the MXene synthesis process. To address this, additional steps are required to eliminate the by-product. Modified etching techniques have demonstrated that $AlF_3{\cdot}3H_2O$ can also form when using cobalt fluorides for etching. These modified approaches improve the interlayer spacing of the resulting MXenes, facilitating intercalation and promoting delamination of the material layers. This refined method streamlines the process by enabling the synthesis of multiple MXene layers in a single step, reducing the time and complexity involved.[9]

**2.1.3. Modified fluoride-based acid etching.** To mitigate the toxicity associated with HF etching, researchers are actively exploring improved methods for removing atomic layers from MAX phases. One common approach involves using a combination of fluoride salts and strong acids for selective etching. This process allows fluoride salts and acids to selectively remove specific atomic layers, leading to the formation of cations. Additionally, introducing water between the MXene layers increases interlayer spacing and reduces their direct contact. However, the concentration of fluoride salts and acids used during the process can significantly impact the quality and size of the resulting MXene fragments. For example, the production of multilayer $Ti_3C_2$ often requires a sonication step to separate the layers into individual flakes when using the clay method. This step, however, can introduce minor defects into the MXene flakes.[10]

**2.1.4. Molten salts etching.** MXenes, including $Ti_4AlN_3$ and other MAX phases, can be synthesized by heating a mixture of molten fluoride salts (*e.g.*, LiF, NaF, KF in a 29 : 12 : 59 wt% ratio) at 550 °C under an argon atmosphere. This etching process can be completed within 30 minutes. It has been observed that TinNn-1 phases are less stable compared to TinCn-1 phases, making them more soluble in HF or other fluoride-based acids used as etchants. As a result, the molten salt etching method offers relatively fast processing times. However, additional steps such as cleaning with deionized water (DI $H_2O$) and $H_2SO_4$, followed by delamination using TBAOH solution, are required to thoroughly remove impurities. The delaminated $Ti_4N_3$ obtained *via* this method exhibits lower crystallinity compared to MXenes produced through HF etching, as indicated by XRD analysis. Moreover, the formation of the $TiO_2$ phase has been noted in the final product. Compared to HF or fluoride-based acid etching, molten salt etching provides the benefit of producing MXenes with limited stability in such acidic environments. However, this method has several drawbacks: (a) it requires significant heat and energy consumption, (b) the resulting MXenes exhibit lower purity and crystallinity, and (c) the final products contain numerous surface defects and voids.[11]

**2.1.5. Etching without fluoride.** The synthesis of MXene materials often relies on the use of HF or fluoride-based chemicals, which result in –O and –F terminations on their surfaces. However, there is increasing interest in developing fluoride-free fabrication methods, as –F terminations have been found to negatively impact the performance of supercapacitors. A notable advancement in this area is the use of NaOH solutions in an alkali-assisted hydrothermal etching process to produce $Ti_3C_2$ MXene.

Achieving high-purity multilayer MXenes has posed challenges, except in cases like the production of $Ti_3C_2$ MXene *via* the Bayer process. Recently, a fluoride-free and chloride-containing $Ti_3C_2T_x$ MXene synthesis method using electrochemical etching has been reported. This approach produces $Ti_3C_2T_x$ nanoflakes through sonication without relying on

 This journal is © The Royal Society of Chemistry 2025

Published on 26 1446. Downloaded on 13/11/47 04:29:14 .

toxic organic intermediates. These findings highlight the growing emphasis on fluoride-free and environmentally friendly techniques for MXene synthesis.[12]

### 2.2. Top-down approaches

The top-down approach is a widely used method for the synthesis and design of nanomaterials. It involves breaking down bulk 2D or 3D materials into smaller quantum-sized particles. This process can produce quantum dots through various techniques, such as ball milling, liquid exfoliation, chemical etching, electrochemical methods, intercalation, hydrothermal or solvothermal treatments, ultrasonication, and microwave irradiation. One of the key benefits of the top-down strategy is its ability to create surface defects on catalysts, which serve as active reactive sites. Additionally, this approach operates at relatively low temperatures and is suitable for large-scale production. However, its drawbacks include low yields and the need for specialized processes. For MXene production, common top-down techniques include ultrasonication, ball milling, intercalation, hydrothermal and solvothermal methods, microexplosion, and acid reflux. The following section will provide a detailed explanation of these methods.[13]

**2.2.1. Hydrothermal approach.** The hydrothermal method is a versatile approach for synthesizing MXenes, utilizing high-temperature (100–180 °C) and high-pressure conditions in an autoclave. Key factors such as reaction temperature, pH (6–9), and duration significantly influence the size, thickness, and properties of the resulting MXenes. For example, $Ti_3C_2$ MXenes produced at 100 °C exhibit monolayer structures, while higher temperatures, like 150 °C, lead to amorphous structures due to increased Ti atom etching. Additionally, heteroatom-doped MXenes, such as S, N-MXene, can be synthesized using precursors like $Nb_2C$ and L-cysteine. This method avoids HF acid, offering a safer, efficient, and environmentally friendly way to produce MXenes with customizable features.[14]

**2.2.2. Solvothermal approach.** The solvothermal process is considered a more straightforward and efficient method for MXene synthesis compared to the hydrothermal approach. In this technique, a non-aqueous organic solvent is used instead of water, allowing for better control over factors such as particle size, dispersion, and crystallinity. As a result, the solvothermal method is seen as more versatile and effective than the hydrothermal method.[15]

**2.2.3. Ball-milling approach.** Ball milling is a top-down technique commonly employed to fabricate quantum dots (QDs) by reducing the size of nanoparticles. The material's physical and morphological properties are influenced by factors such as the type of grinding (wet or dry), milling speed, the ratio of ball to powder weight, and the duration of the grinding process. This method is particularly effective for producing nanocomposites.[16]

**2.2.4. Ultrasonic approach.** The ultrasonic method is an environmentally friendly technique for producing MXene quantum dots (MQDs). It works by using acoustic cavitation, where bubbles form within a liquid medium, breaking down materials into QDs while maintaining their inherent characteristics. Solvents with high boiling points and surface energies, such as DMSO, DMF, and TBAOH, help disperse bulk materials into smaller, well-dispersed QDs. For example, Yu *et al.*[17] employed TBAOH-assisted exfoliation and ultrasonication to synthesize $Ti_3AlC_2$ MXene QDs. Additionally, combining ultrasonication with hydrothermal or solvothermal processes has been shown to improve yield and decrease processing time.[17]

### 2.3. Bottom-up approaches

Bottom-up methods use molecular materials as starting points to produce MQDs, unlike top-down techniques that rely on bulk materials. These methods offer benefits such as higher atomic efficiency, better control over structural and morphological aspects, faster functionalization, and improved properties. However, challenges remain in scaling up production with efficient, low-toxicity precursors, mild reaction conditions, high crystallinity, monodispersity, and high yields. Although more research is needed in this area for MQD fabrication, one-pot bottom-up techniques are expected to gain prominence for MXene production due to their simpler and more efficient process.[18]

**2.3.1. Pyrolysis approach.** Pyrolysis is a promising bottom-up technique for synthesizing MQDs due to its simplicity, low environmental impact, and high yield. For example, $Mo_2C$ QD-carbon polyhedron composites were created by pyrolyzing Mo/ZIF-8 at 700 °C for 2 hours in an argon environment, resulting in a uniform distribution of ultra-small $Mo_2C$ dots within the carbon matrix. While pyrolysis is an effective method, additional research is required to refine and scale up these synthesis techniques for commercial use. Key factors influencing the synthesis process include reaction time, temperature, precursor concentration, and the choice of elements. MXenes like $Ti_3C_2T_x$ display excellent electrocatalytic properties, owing to their metallic conductivity and surface functional groups.[16]

## 3. MXenes in pathogen detection and biosensing

The design of advanced MXene-based biosensors holds significant potential to revolutionize pathogen detection, clinical diagnostics, disease monitoring, and drug discovery (Table 1). MXenes, as a class of two-dimensional materials, exhibit exceptional properties such as high biocompatibility, large surface area, excellent mechanical and thermal properties, superior electrical conductivity, and outstanding chemical stability.[19] These characteristics make MXenes ideal candidates for developing biosensors with high sensitivity and selectivity for detecting pathogenic viruses and bacteria (Table 1). The extensive surface area and hydrophilic nature of MXenes enable efficient immobilization of biomolecules, while their electrical conductivity and stability enhance signal transmission.[20] Furthermore, MXene-based biosensors not only detect pathogens with high sensitivity and precision but

Published on 26 1446. Downloaded on 13/11/47 04:29:14 .

also exhibit antimicrobial properties that inactivate viruses and bacteria. These features make them particularly attractive for fabricating advanced diagnostic tools. MXenes have been effectively utilized in various biosensing applications, including ultrasensitive detection of biomarkers and pathogens essential for clinical diagnostics. As electroactive bio interfaces, MXene-based nanocomposites function as efficient bioreceptors, electrochemical transducers, and amplification probes. These capabilities allow the transformation of molecular recognition events into detectable signals, paving the way for the development of next-generation biosensors. Studies emphasize the influence of synthesis methods, surface chemistry, and nanocomposite design on the electrochemical properties and performance of MXene-based biosensors. The integration of MXenes into biosensing platforms enhances their ability to selectively and sensitively detect nucleic acids, proteins, and pathogens, which are crucial for molecular diagnostics. Despite ongoing challenges in optimizing biosensor performance, research continues to expand their applications to other fields, reinforcing their role in advancing early disease detection and clinical diagnostics. In summary, the unique combination of properties exhibited by MXenes positions them as transformative materials in biosensor technology. Ongoing research and development efforts aim to optimize their performance and broaden their applications, ensuring their significant contribution to healthcare and biotechnology advancements.[21,22]

MXenes, particularly transition metal carbide/nitride-based two-dimensional (2D) materials such as $Ti_3C_2T_x$, exert their antimicrobial activity against bacteria and fungi through a synergistic combination of physical, chemical, and biochemical mechanisms. Physical membrane damage arises from the direct interaction of MXenes' atomically sharp edges and ultrathin lamellar structure with microbial cell membranes. For instance, in bacteria, these sharp nanostructures mechanically penetrate the thick peptidoglycan layer of Gram-positive species or the lipopolysaccharide (LPS)-rich outer membrane of Gram-negative species. In fungi, MXenes disrupt structural integrity by breaching chitin- and β-glucan-containing cell walls. The high surface area and interlayer flexibility of MXenes optimize this penetration, while their nanoblade-like edges induce irreversible tearing of the lipid bilayer, leading to cytoplasmic leakage and cell lysis.

Oxidative stress is triggered by the catalytic activity of MXenes' metallic components (*e.g.*, Ti, Mo) and surface functional groups (–O, –OH). This process generates reactive oxygen species (ROS), including superoxide anions ($O_2^-$), hydroxyl radicals ($^{\bullet}OH$), and hydrogen peroxide ($H_2O_2$). ROS induce lipid peroxidation in membranes, oxidize sulfhydryl (–SH) groups in critical enzymes, and cause DNA strand breaks, thereby crippling cellular metabolic functions. In fungi, ROS-mediated inhibition of ergosterol biosynthesis further compromises membrane permeability and ion homeostasis. The ROS generation capacity of MXenes is modulated by factors such as particle size, surface chemistry, and environmental pH.

Electrostatic interactions occur between the negatively charged surface of MXenes (due to –O, –OH, or –F terminations) and the positively charged microbial cell membranes (*e.g.*, bacterial lipoteichoic acids or fungal chitosan-rich walls). This attraction accelerates MXene adsorption onto cell surfaces, creating localized electrostatic imbalances. Consequently, membrane potential collapses, ion channels (*e.g.*, $K^+$, $Ca^{2+}$) open uncontrollably, and plasmolysis ensues due to osmotic pressure loss. In fungi, this disrupts hyphal growth and spore formation.

MXenes also impair microbial resilience by inhibiting biofilm formation. Interactions between MXenes and extracellular polymeric substances (EPS) in the biofilm matrix reduce microbial adhesion. Surface modifications, such as silver nanoparticle functionalization, enhance antimicrobial efficacy by promoting intracellular metal ion release. In fungi, MXenes suppress cell wall synthesis enzymes (*e.g.*, chitin synthase) and collapse mitochondrial membrane potential, inducing apoptosis-like cell death.

Environmental factors further modulate MXene efficacy: lower pH enhances electrostatic attraction by increasing surface positive charge, while light exposure (photothermal effect) generates localized heat, destabilizing membranes and denaturing proteins. The dynamic interplay of these mechanisms ensures broad-spectrum activity, even against resistant pathogens.

Visualization strategies to elucidate these processes include:

- TEM/SEM imaging: capturing real-time membrane penetration events,
- Fluorescence assays: detecting intracellular ROS using probes like DCFH-DA,
- Zeta potential analysis: quantifying surface charge interactions,
- 3D biofilm models: demonstrating EPS matrix disruption.

This multilayered mechanistic profile underscores MXenes' superiority over conventional antimicrobials and highlights their potential as next-generation smart materials for combating drug-resistant infections.[6]

### 3.1. Mechanisms of pathogen detection in MXene-based biosensors

A study on the use of various nanomaterials in electrochemical biosensors for pathogen detection was conducted.[51] The incorporation of nanomaterials, including 2D materials such as MXenes, has been shown to enhance the sensitivity and reproducibility of electrochemical biosensors.[52] The association of nanomaterials with electrodes increases the surface area, which improves mass transport and loading capacities, resulting in amplified signals.[53] Nanomaterials, especially 2D MXenes, are advantageous in electrochemical biosensing due to their high surface-to-volume ratio, tunable electronic properties, and excellent mechanical strength.[54] MXenes and other 2D nanomaterials, such as graphene, have been recognized for their potential in detecting foodborne pathogens and improving biosensor performance. Additionally, nanomaterials

 This journal is © The Royal Society of Chemistry 2025

Published on 26 1446. Downloaded on 13/11/47 04:29:14 .





**Table 1** MXene-based biosensors for pathogen detection, highlighting their sensitive layers, target biomarkers, detection limits (LOD), and the strategies applied for various bacterial and viral pathogens. The Strategies column includes methods for using MXene in biosensors, antimicrobial coatings, and other medical applications

| Pathogen/bacteria/virus | Detection methods | Biosensor type | Sensitive layer | Target biomarker | LOD | Treatment methods | MXene applications | Implementation strategies | Ref. |
|---|---|---|---|---|---|---|---|---|---|
| Listeria monocytogenes | PCR, ELISA, Biosensors | Electrochemical | MXene-$Ti_3C_2T_x$ nanosheets | Internalin A | 10 CFU $mL^{-1}$ | Antibiotics (ampicillin, gentamicin) | MXene-based biosensors for rapid detection, antibacterial coatings | Surface modification of MXenes | 6 and 23 |
| *Staphylococcus aureus* (MRSA) | PCR, immunoassays, Lateral flow assays | Electrochemical | MXene-Ag nanocomposites | mecA gene | 1 CFU $mL^{-1}$ | Antibiotics (vancomycin, linezolid) | MXene-based photothermal ablation, electrochemical biosensors | Photothermal therapy, antibiotic resistance monitoring | 24 and 25 |
| Salmonella | PCR, ELISA, Lateral flow assays | Fluorescent | MXene-fluorescent quantum dots | invA gene | 5 CFU $mL^{-1}$ | Antibiotics (ciprofloxacin, azithromycin) | MXene-based electrochemical sensors for Salmonella detection | Nano-enhanced fluorescence | 26 and 27 |
| SARS-CoV-2 | PCR, antigen tests, Immunoassays | Electrochemical | MXene-AuNP composites | Spike protein, RNA | 100 fg $mL^{-1}$ | Antiviral drugs (remdesivir), vaccines | MXene-based biosensors for virus detection, photothermal virus inactivation | Enhanced conductivity for viral RNA detection | 28 and 29 |
| *Escherichia coli* (*E. coli*) | PCR, ELISA, Biosensors | Optical | MXene-SERS substrates | O157:H7 | 1 CFU $mL^{-1}$ | Antibiotics (ampicillin, nitrofurantoin) | MXene-coated electrodes for electrochemical detection | Surface-Enhanced Raman spectroscopy (SERS) | 30 and 31 |
| Human papillomavirus (HPV) | PCR, ELISA, DNA sequencing | Electrochemical | MXene-graphene composites | E6/E7 oncogenes | 10 pg $mL^{-1}$ | Vaccination (Gardasil, Cervarix) | MXene-based nanostructures for viral DNA detection | Nucleic acid sensing | 32 and 33 |
| Influenza Virus | PCR, antigen tests, Lateral flow assays | Electrochemical | MXene-AuNP composites | Hemagglutinin protein | 100 fg $mL^{-1}$ | Antiviral drugs (oseltamivir, zanamivir) | MXene-based virus detection devices | Conductive layer optimization | 34 and 35 |
| *Bacillus subtilis* | PCR, biosensors, microscopy | Fluorescent | MXene-functionalized graphene | DNA fragments | 50 CFU $mL^{-1}$ | Antibiotics (tetracycline, penicillin) | MXene biosensors for detection and electrical conductivity measurements | Optical enhancement strategies | 36 and 37 |
| *Enterococcus faecalis* | PCR, ELISA, Agar plate tests | Electrochemical | MXene-polymer nanohybrids | Vancomycin-resistant genes | 10 CFU $mL^{-1}$ | Antibiotics (ampicillin, vancomycin) | Structural modifications with MXenes, biosensors for antibiotic resistance detection | Resistance gene monitoring | 38 and 39 |
| *Klebsiella pneumoniae* | PCR, ELISA, Blood cultures | Fluorescent | MXene-$SiO_2$ nanocomposites | KPC gene | 5 CFU $mL^{-1}$ | Antibiotics (cefotaxime, meropenem) | MXene biosensors for rapid identification and monitoring | Fluorescence quenching | 40 |
| Vibrio parahaemolyticus | PCR, ELISA, Immunoassays | Electrochemical | MXene-CdS nanostructures | tdh gene | 10 CFU $mL^{-1}$ | Antibiotics (doxycycline) | MXene-based sensors for waterborne pathogens | Multi-target detection | 41 and 42 |
| Vibrio spp. | PCR, Biosensors, Microscopy | Fluorescent | MXene-functionalized nanodots | ctxA gene | 5 CFU $mL^{-1}$ | Antibiotics, Probiotics | MXene-based microfluidic systems for bacterial tracking | Multi-spectral fluorescence detection | 43 and 44 |

This journal is © The Royal Society of Chemistry 2025

Published on 26 1446. Downloaded on 13/11/47 04:29:14 .

**Table 1** *(Contd.)*

| Pathogen/bacteria/virus | Detection methods | Biosensor type | Sensitive layer | Target biomarker | LOD | Treatment methods | MXene applications | Implementation strategies | Ref. |
|---|---|---|---|---|---|---|---|---|---|
| Norovirus | PCR, Immunoassays, ELISA | Electrochemical | MXene-polymer composites | VP1 protein | 100 pg $mL^{-1}$ | Supportive care, Vaccines (in development) | MXene-based biosensors for fecal contamination detection | Flexible and portable sensors | 45 |
| Rotavirus | PCR, Immunoassays, VP6 Antigen Tests | Electrochemical | MXene-embedded polymers | VP6 protein | 1 ng $mL^{-1}$ | Vaccines (Rotarix, RotaTeq) | MXene-based immunosensors for VP6 antigen detection | Low-cost rapid detection systems | 46 and 47 |
| SERS Pathogens | Surface-Enhanced Raman Spectroscopy (SERS) | Optical | MXene-SERS substrates | Raman-active pathogens | 1 CFU $mL^{-1}$ | Antibiotics, Antimicrobials | MXene-enhanced SERS substrates for pathogen detection | Raman spectroscopy enhancement | 48 and 49 |
| *Helicobacter pylori* | PCR, Urea Breath Test, Endoscopy | Electrochemical | MXene-based urease inhibitors | Urease enzyme | 100 fg $m^{-1}L$ | Antibiotics (amoxicillin, clarithromycin) | MXene-based sensors for rapid urease activity detection | Enzyme-based biosensing | 50 |

such as gold nanoparticles and quantum dots, often combined with MXenes, have been explored to improve signal detection and enhance the overall functionality of biosensing platforms. These advancements highlight the promising role of MXenes in pathogen detection, offering both high sensitivity and selectivity for biosensing applications.[55]

The use of MXenes in pathogen detection and biosensing has been explored through various studies. One notable example is the development of a multifunctional signal-amplifying tag for the detection of *Vibrio parahaemolyticus (V.P.)*, a common foodborne pathogen. The signal amplification was achieved through the complexation of $Ti_3C_2$ MXene with gold nanobipyramids (AuNBPs), followed by functionalization with an antimicrobial peptide (AMP) and conjugation with a DNAzyme probe.[56] This system enabled dual recognition of V. P. using both fluorescence and electrochemical signals. The results indicated that the biosensor could effectively detect V.P. with a concentration range from 10 to $10^8$ CFU $mL^{-1}$.[57]

In a study, a dual-mode biosensor combining photoelectrochemical (PEC) and surface-enhanced Raman scattering (SERS) was developed for the detection of *Staphylococcus aureus* (*S. aureus*). The biosensor employed a dual-recognition strategy based on DNA walking and utilized a carbon nitride nanosheet ($C_3N_4$)/MXene–gold nanoparticle (C/M–Au NPs) hybrid as the accelerator. The $C_3N_4$ and MXene materials self-assembled electrostatically to form a photoactive heterostructure, and the *in situ* growth of gold nanoparticles enhanced both PEC and SERS performance. A DNA walking mechanism, dependent on $Pb^2$+-activated DNAzyme, enabled dual recognition. In the presence of *S. aureus*, intermediate DNA (I-DNA) was generated, triggering the opening of methylene blue-tagged hairpin DNA (H-MB) on the electrode surface. The aim of the study was to achieve more sensitive and accurate detection of *S. aureus* by combining PEC and SERS for mutual result validation in a single reaction. Experimental results demonstrated detection limits of 0.70 CFU $mL^{-1}$ (PEC) and 1.35 CFU $mL^{-1}$ (SERS) with wide detection ranges, highlighting the potential of MXene-based biosensors in advancing biosensing technologies.[58]

A study has been conducted to develop a rapid, one-step electrochemical sensor for the detection of foodborne pathogens such as *Escherichia coli* (*E. coli*), *Staphylococcus aureus (S. aureus)*, and *Salmonella typhimurium (S. typhimurium)*. The sensor utilizes aptamer, carboxylate $Ti_3C_2T_x$ (C-$Ti_3C_2T_x$), and Zn-MOF composites to integrate recognition elements, signal tags, and amplifiers on the electrode surface. The aptamers selectively capture pathogens, leading to an increase in the impedance of the electrode surface and a decrease in the current of Zn-MOF, enabling rapid bacterial quantification through a one-step detection method. The detection limits for *E. coli*, *S. aureus*, and *S. typhimurium* were found to be 6, 5, and 5 CFU $mL^{-1}$, respectively. The sensor demonstrated reliable performance in real-sample testing. This study highlights the potential of MXene-based two-dimensional composites for pathogen detection and biosensing applications in food safety, providing valuable insight into the development of MXene-based biosensors.[59]


This journal is © The Royal Society of Chemistry 2025

Published on 26 1446. Downloaded on 13/11/47 04:29:14 .

The accurate detection of pathogens, such as infectious bacteria, is considered a critical step for the timely treatment of infectious diseases globally. Recent advancements in 2D materials have significantly contributed to the development of biosensors capable of rapid and accurate pathogen detection in clinical diagnostics. In one study,[60] nitrogen-doped MXene (NMXene) modified with mannose (Man) was developed through hydrothermal treatment of $Ti_3C_2T_x$ MXene nanosheets with urea, followed by the physical adsorption of D-(+)-mannose. This modification aimed at targeting FimH proteins commonly found on the tip of *E. coli* bacteria. The detection principle, based on Electrochemical Impedance Spectroscopy (EIS), was founded on the reduction of accessibility of redox probes ($Fe^{2+}/Fe^{3+}$) to the NMXene-Man working electrode, caused by the blocking of the solid–liquid interface by the larger *E. coli* bacteria. The sensitivity of the biosensor was validated by a linear response of the change in charge transfer resistance ($\Delta R_{ct}$) against the increasing concentration of *E. coli* from 10 to $10^8$ CFU $mL^{-1}$. Notably, the NMXene-Man-based biosensor exhibited a high selectivity for *E. coli* detection, demonstrating the highest $\Delta R_{ct}$ compared to other bacterial strains, such as *A. baumannii* and *S. aureus*, at the same concentration of $10^7$ CFU $mL^{-1}$. This research highlights the potential of MXene-based biosensors for specific pathogen detection, particularly in addressing foodborne *E. coli* infections.[60]

Furthermore, the development of other biosensors using advanced materials, such as an electrochemical sandwich assay utilizing AuNP-functionalized carbon nanotubes combined with anti-*E. coli* antibodies and platinum-nickel[61] alloy nanoparticles, has further enhanced pathogen detection efficiency. This biosensor achieved a sensitivity of 38 CFU $mL^{-1}$ with a linear detection range of 150–$1.5 \times 10^7$ CFU $mL^{-1}$ for *E. coli*. These findings suggest that MXene-based biosensors could outperform other types of biosensors in the detection of *E. coli*, with significant potential for widespread application in clinical diagnostics and pathogen monitoring (Fig. 1A).[22]

Additionally, an electrochemical biosensor functionalized with $Ti_3C_2$ MXene has been developed for the detection of the H1N1 influenza virus. The probe, formed by coupling glucose oxidase (GOx) with polyclonal anti-H1N1 antibodies, was used in a sandwich immunoassay. The system showed an impressive dynamic range and high sensitivity in detecting the virus, with a concentration range from 0.01 to 100 μg $mL^{-1}$, as determined by pH reduction due to glucose conversion. Both studies highlight the significant potential of MXene-based biosensors in detecting pathogens, with improvements in sensitivity, selectivity, and dynamic range, making them promising candidates for future diagnostic applications in microbiology and virology[22,67] (Fig. 1B).

Li *et al.*[68] developed an MXene–graphene field-effect transistor (FET) sensor for detecting both influenza virus and 2019-nCoV. The sensor combines the high sensitivity of MXene and graphene to form a virus-sensing material, utilizing antibody–antigen binding for electrochemical signal transduction. Integrated into a microfluidic channel, the sensor detected varying concentrations of inactivated influenza A (H1N1) HA virus (125–250 000 copies per mL) and recombinant 2019-nCoV spike protein (1 fg $mL^{-1}$–10 pg $mL^{-1}$). The response time was ~50 ms, much faster than RT-PCR (>3 hours). With detection limits of 125 copies per mL (influenza) and 1 fg $mL^{-1}$ (2019-nCoV), the sensor demonstrated excellent sensitivity, high signal-to-viral load ratio, and specificity. The results indicate the sensor's potential for rapid, sensitive, and specific virus detection in medical diagnostics.[68]

A study conducted by Chen *et al.*[69] focused on the development of MXene-based biosensors for the detection of viral pathogens. In this work, a DNA-functionalized MXene-based chemoresistive biosensor was introduced for the selective and rapid detection of the nucleocapsid gene of SARS-CoV-2.[69] The biosensing platform was fabricated through the non-covalent adsorption of probe DNA molecules onto two-dimensional $Ti_3C_2T_x$ MXene. Upon hybridization between the complementary gene of SARS-CoV-2 and the probe single-stranded DNA (ssDNA) immobilized on the MXene surface, an increase in the conductance of the sensing channel was observed. In contrast, no response was detected for non-complementary targets, such as the SER-CoV-1 N gene and MER-CoV N gene, demonstrating the high selectivity of the biosensor. The study reported that the biosensor achieved a detection limit (LOD) below $10^5$ copies/mL in saliva, comparable to the sensitivity of RT-PCR.

The importance of rapid pathogen detection for effective disease management has gained prominence, especially in light of the COVID-19 outbreak, which underscored the need for early detection. Traditional diagnostic methods, such as bacterial culture, PCR, and ELISA, are time-consuming and costly. In contrast, biosensors offer higher accuracy, sensitivity, selectivity, stability, and lower costs with simpler operations. MXenes, with their excellent electrical conductivity, ease of functionalization, and ion-intercalation properties, make ideal candidates for biosensor development, offering high specificity and performance in detecting viruses and bacteria.[70]

Recent advancements in MXene-based biosensors have demonstrated significant potential in pathogen detection. For instance, an aptamer-based surface plasmon resonance (SPR) biosensor was developed to detect the SARS-CoV-2 N gene. In this study, thiol-modified niobium carbide MXene quantum dots were employed to immobilize an N-gene-specific N58 aptamer. The biosensor exhibited a linear detection range of $5 \times 10^{-2}$ to 100 ng $mL^{-1}$ and achieved a limit of detection (LOD) of 4.9 pg $mL^{-1}$.[65] The combination of MXenes with metal–organic frameworks (MOFs) has also been investigated to enhance their electrical conductivity. Wang *et al.*[71] developed an electrochemiluminescence (ECL)[72] biosensor for screening HIV-1, integrating $Ti_3C_2T_x$ MXene with a ZIF-8 MOF. The biosensor, functionalized with ssDNA, carbon black, and magnetic nanoparticles, achieved a linear detection range of 1 fM to 1 nM and a LOD of 0.3 fM for HIV-1 protein detection. Furthermore, Peng *et al.*[26] designed a fluorescent biosensor to monitor HPV-18 infection, utilizing ultrathin MXene

Published on 26 1446. Downloaded on 13/11/47 04:29:14 .

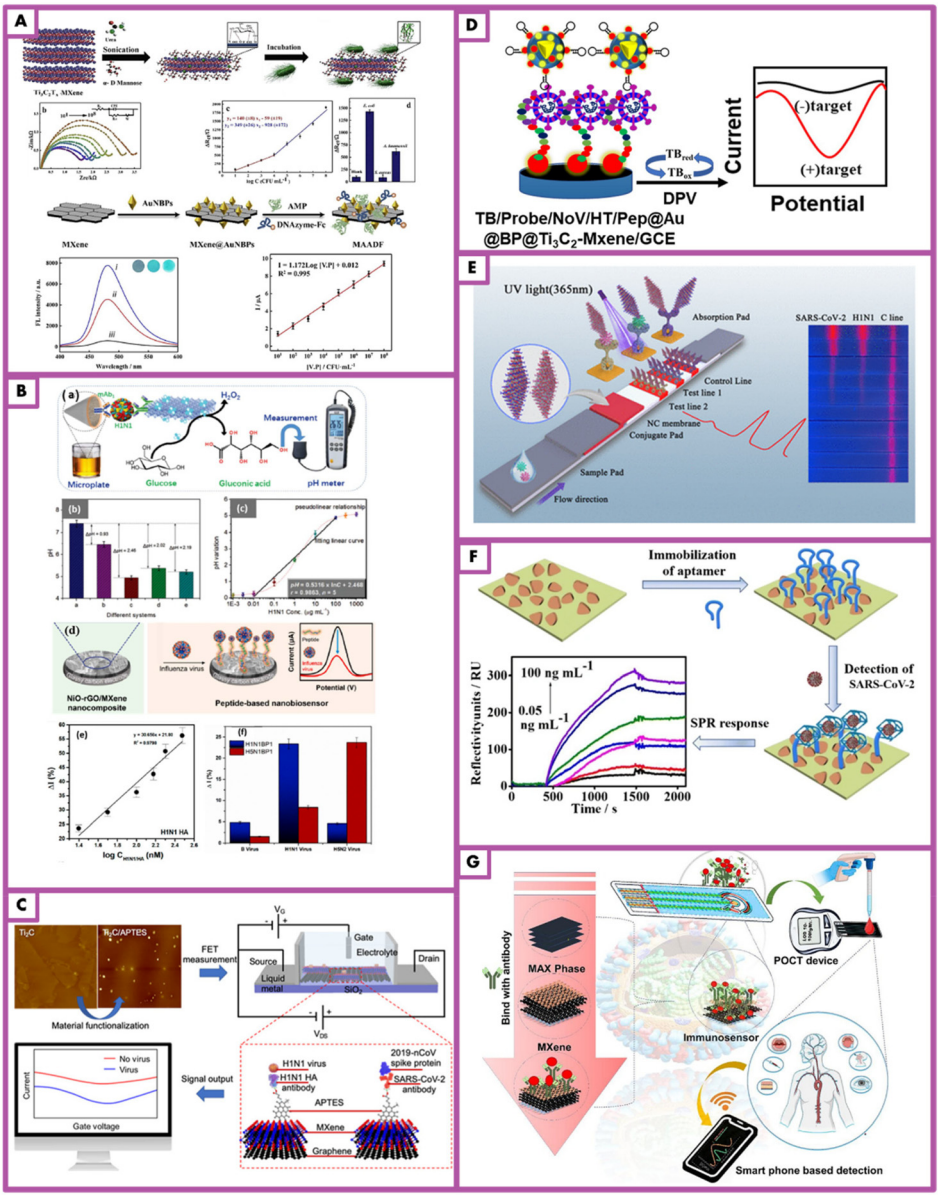


**Fig. 1** (A) Schematic overview: (a) the development of a bacteria biosensor through multivalent hydrogen bonding between MXene's surface moieties and mannose for detecting *E. coli*. (b) The correlation between the observed changes in interfacial resistance and varying *E. coli* concentrations (ranging from $10^1$ to $10^8$ CFU mL$^{-1}$). (c) The corresponding linear calibration curve of $\Delta R_{ct}$ as a function of the logarithm of *E. coli* concentration. (d) EIS measurement illustrating the selectivity of the NMXene-Man biosensor for *E. coli* detection among three different bacterial strains. (e) The use of multifunctional MXene-based nanocomposite tags to generate both fluorescent and electrochemical dual-signal responses in the biosensor for precise V.P. detection. (f) Fluorescence excitation/emission spectra in response to DNAzyme-catalyzed azide–alkyne cycloaddition: (i) without V.P, (ii) with $10^5$ CFU mL$^{-1}$ V.P, and (iii) with $10^8$ CFU mL$^{-1}$ V.P on an MAADF-based biosensor. (g) SWV responses for V.P. detection and the corresponding linear relationship on the MAADF-based biosensor in PBS reproduced from ref. 22. (B) Schematic summary includes the following: (a) the principle of a pH meter-based immunoassay for detecting H1N1 influenza virus, using the GOx-$Ti_3C_2$-pAb2 probe, where immobilized GOx enzyme converts glucose to gluconic acid, resulting in a pH decrease. (b) pH responses from the developed immunoassay using different 2D material-based signal labels. (c) The correlation between pH change and H1N1 virus concentration, detected by the pH meter using the GOx-$Ti_3C_2$-$pAb_2$ probe. (d) Fabrication of a NiO-rGO/MXene nanocomposite-based peptide biosensor for detecting H1N1 virus and viral proteins. (e) Calibration curves for detecting H1N1 HA antigen concentration in human blood plasma using the BP1-NiO-rGO/MXene working electrode. (f) Selectivity of the BP1-NiO-rGO/MXene electrode for H1N1 virus detection among various viruses (H1N1, H5N2, and B) reproduced from ref. 22 (C) Schematic summary, the MXene-graphene FET sensor is shown for rapid and sensitive detection of influenza A and 2019-nCoV with low detection limits.[62] Copyright 2021 American Chemical Society. (D) Schematic summary, the electrochemical biosensor developed with Au@BP@$Ti_3C_2$-MXene and Au@$ZnFe_2O_4$@COF nanocomposites is shown.[63] Copyright 2023 Elsevier. (E) The schematic summary shows the $Ti_3C_2$-QD-ICA biosensor developed for rapid detection of influenza A (FluA) and SARS-CoV-2.[64] Copyright 2023 American Chemical Society. (F) Schematic summary, Nb2C-SH QD-based SPR aptasensor detects SARS-CoV-2 N-gene with high sensitivity and has been shown to exhibit selectivity in different samples.[65] Copyright 2021 SPRINGER NATURE (G) Schematic summary shows that MXene-based biosensors can enhance pandemic preparedness by offering high sensitivity, speed and low cost in virus detection.[66] Copyright 2024 Elsevier .


This journal is © The Royal Society of Chemistry 2025

Published on 26 1446. Downloaded on 13/11/47 04:29:14.

nanosheets, dye-labeled ssDNA probes, and exonuclease III. This sensor was shown to detect HPV ssDNA at picomolar levels with a linear response ranging from 0.5 nM to 50 nM.[71]

Recently, significant advancements have been made in developing MXene-based biosensors for detecting pathogenic bacteria. In one such study, a biosensor for the detection of *Mycobacterium tuberculosis* (*M. tuberculosis*)[73] was developed using peptide nucleic acid (PNA) as a capture probe and zirconium-linked $Ti_3C_2$ MXene as a signal amplifier. The PNA probe was immobilized on a gold electrode, where the hybridization of *M. tuberculosis*-specific biomarkers with PNA enhanced the conductance of the MXene-modified electrode. This biosensor demonstrated the ability to discriminate among multiple bacterial species, including *Escherichia coli*, *Pseudomonas aeruginosa*, *M. tuberculosis*, and *Staphylococcus aureus*, while offering reusability up to six cycles.[74]

Another study presented an accordion-like $Ti_3C_2T_x$ MXene-based electrochemical DNA biosensor capable of detecting *Helicobacter pylori* target DNA at femtomolar concentrations. Additionally, an MXene-based dual-mode ECL and surface-enhanced Raman scattering (SERS) biosensor was designed for detecting *Vibrio vulnificus* (VV). In this design, multifunctional MXene nanoparticles ($R_6G$-$Ti_3C_2T_x$@AuNRs) functionalized with ECL signal tags and VV-specific antibodies enabled detection limits of 1 CFU $mL^{-1}$ *via* ECL and 102 CFU $mL^{-1}$ *via* SERS.[75] These findings collectively highlight the versatility and potential of MXene-based biosensors in pathogenic detection applications, offering high sensitivity, specificity, and reusability.[21]

In previous research, an innovative electrochemical sensor was developed for the detection of *Listeria monocytogenes* (LM), one of the most hazardous pathogens associated with severe diseases. This sensor was constructed by utilizing $Ti_3C_2T_x$ MXene nanoribbons ($Ti_3C_2T_xR$) as a carrier and thionine (Th), which simultaneously served as a signal probe and functional monomer. The pathogen-imprinted polymer (PIP) was formed through the electropolymerization of Th on the $Ti_3C_2T_xR$-modified glassy carbon electrode (GCE) surface in the presence of LM. Following the removal of template LM cells from the imprinted cavities, the fabricated PIP/$Ti_3C_2T_xR$/GCE sensor demonstrated effective rebinding to LM cells. The detection mechanism was based on the weakening of the Th signal peak current upon the rebinding of LM cells, with the absolute change in current correlating to LM concentration.

This approach resulted in a highly sensitive sensor with a detection limit as low as 2 CFU $mL^{-1}$ and a broad linear range from 10 to $10^8$ CFU $mL^{-1}$. Additionally, the sensor exhibited excellent selectivity, reproducibility, and stability, highlighting its potential in pathogen detection. These findings emphasize the utility of MXene-based materials in designing advanced biosensors for sensitive and selective detection of bacterial pathogens, particularly in microbiological and clinical applications.[76]

The detection of pathogenic bacteria, particularly Methicillin-resistant *Staphylococcus aureus* (MRSA), presents critical diagnostic challenges due to the high morbidity rates associated with these microorganisms. In a study, a magnetic separation-based electrochemical biosensor was developed for MRSA detection. Polyethyleneimine (PEI)-mediated magnetic beads (MBs) were modified with vancomycin (Van) to create MBs-PEI-Van, enabling the separation and enrichment of MRSA. The MBs-PEI-Van demonstrated satisfactory stability and applicability, achieving a capture efficiency exceeding 85% in phosphate-buffered saline (PBS) and cerebrospinal fluid (CSF) samples.

Furthermore, MXene@Au nanocomposites, containing gold nanoparticles (AuNPs) of controllable size synthesized through a self-reduction method, were used to modify a glassy carbon electrode (GCE). Immunoglobulin G (IgG) was immobilized on the modified electrode to bind MRSA, while ferroceneboronic acid (Fc-BA) served as a probe for quantitative detection. Differential pulse voltammetry (DPV) revealed a correlation between the DPV current and MRSA concentrations as low as $3.8 \times 10$ CFU $mL^{-1}$. In spiked CSF samples, the biosensor achieved satisfactory recovery rates ranging from 94.35% to 107.81%, with a relative standard deviation (RSD) below 11%.[36]

### 3.2. MXene-based electrochemical sensors for microbial detection

In recent years, the development of ultrasensitive electrochemical biosensors has progressed significantly, particularly with the use of carbon-based nanomaterials, such as carbon nanotubes, followed by metal oxide nanoparticles and 2D materials. The exceptional electrical, interfacial, and optical properties of 2D materials have been effectively utilized to enhance biosensor performance.[77–79] This includes the rapid advancements in electrochemical biosensor technology, which are driven by the versatile and outstanding characteristics of 2D materials, facilitating the design and fabrication of highly selective sensory elements for working electrodes.[80,81] Recent research has shown a growing interest in the application of MXenes as bioreceptors or transducers in electrochemical biosensors, driven by their ease of synthesis, fabrication, and functionalization. These two-dimensional materials have demonstrated high biocompatibility, making them ideal for the incorporation of biomacromolecules, such as proteins and nucleic acids, on electrochemical biointerfaces. Consequently, MXenes provide a suitable platform for molecular recognition, electrochemical reactions, and signal amplification, which are critical for the effective functioning of electrochemical biosensors. Despite the decade-long exploration of MXenes in various established fields, there remains a lack of comprehensive reviews focusing on their emerging applications in electrochemical biosensing. A recent study provides a systematic overview of MXene-based electrochemical biosensors developed between 2020 and 2023 for detecting specific targets, including nucleic acids, proteins, and pathogens. The research underlines the potential of MXenes for the ultrasensitive detection of these targets and emphasizes their importance in the advancement of electrochemical biosensors for pathogen detection.[22]

Published on 26 1446. Downloaded on 13/11/47 04:29:14 .

*Vibrio vulnificus (VV)* is a Gram-negative bacterium, widely found in estuaries, bays, coastal waters, and marine animals, which can pose serious health risks to humans.[82] VV is one of the most lethal species within the Vibrio genus, associated with acute gastroenteritis, primary sepsis, necrotizing wound infections, and even death. Given the potential threat posed by this bacterium, rapid, sensitive, and accurate on-site detection methods are crucial for monitoring seawater and seafood.

Detection methods for pathogenic bacteria like VV are categorized into three main types:

1. Traditional microbial culture methods: these involve cultivating bacteria using selective media and detecting them through techniques such as the most probable number method, colony counting, or membrane filtration. While these methods are highly accurate, they rely on the slow growth and reproduction of bacteria, which makes them time-consuming.[83]

2. Immunological methods: these methods leverage immune reactions between the target bacteria and specific antibodies for detection, including enzyme-linked immunosorbent assays (ELISA), immunofluorescence assays (IFA), and serum neutralization tests (SNTs). While these methods are fast and accurate, their sensitivity is often insufficient for detecting bacteria at low concentrations, which is crucial for food and medical applications.[84]

3. Genomics-based methods: these methods utilize the unique genetic characteristics of each bacterium for detection. Techniques such as polymerase chain reaction (PCR), droplet digital PCR, multiplex PCR, real-time PCR, and microarrays are used for this purpose. These methods are sensitive and accurate but require large equipment, skilled operators, and are expensive, which limits their applicability in rapid on-site testing.[85]

These conventional methods are effective but are often slow, labor-intensive, and costly for on-site pathogen detection in environmental and clinical settings. In contrast, MXene-based electrochemical biosensors hold great promise for providing fast, sensitive, and cost-effective detection of pathogenic bacteria in various samples. This technology is highly relevant for the future development of portable, on-site pathogen detection systems in fields such as microbiology and food safety.

In a similar study, a new method to improve the performance of electrochemical biosensors for pathogen detection was proposed.[86] Conventional sandwich-type biosensor designs face difficulties when detecting larger targets such as pathogens due to the increased distance between the electrochemical signal labels and the electrode surface. This results in reduced detection sensitivity. To overcome this problem, a Faraday cage-type electrochemical immunosensor design using 2D conductive materials such as MXenes to label electrochemical signal tags is introduced. This design significantly improves the detection sensitivity by reducing the distance between the signal labels and the electrode surface, thus increasing the possibility of electron tunnelling. MXenes, with their excellent conductivity, serve as an integral part of the electrode, facilitating more efficient electron transfer and improving the overall performance of the sensor in the detection of microbial pathogens.[87]

A study developed a MXene-graphene field-effect transistor (FET) sensor for the detection of both influenza virus and 2019-nCoV. The sensor utilizes the high chemical sensitivity of MXene and the continuous large-area structure of graphene, creating an ultra-sensitive virus-sensing transduction material (VSTM). The sensor operates by utilizing antibody–antigen binding for electrochemical signal transduction, achieved when viruses bind to the VSTM surface.

The sensor was integrated into a microfluidic channel, allowing it to directly receive viruses in solution. The performance was tested with various concentrations of two viruses: inactivated influenza A (H1N1) and recombinant 2019-nCoV spike protein. The sensor demonstrated exceptional sensitivity, with limits of detection of 125 copies per mL for influenza virus and 1 fg $mL^{-1}$ for the 2019-nCoV spike protein, and an average response time of approximately 50 ms, significantly faster than conventional PCR methods. The high signal-to-viral load ratio further indicated the ultra-sensitivity of the developed sensor. Additionally, the sensor exhibited good specificity, as evidenced by the differential responses when testing with opposite antibodies for the two viruses[62] (Fig. 1C).

In this similar study, an electrochemical biosensor was developed using conductive $Ti_3C_2$ MXenes for the detection of *Mycobacterium tuberculosis (M. tuberculosis)*. The sensor employed a species-specific fragment of ssDNA located in the 16S rDNA of *M. tuberculosis* as the target biomarker. The PNA (Peptide Nucleic Acid) was utilized as a capture probe, and a $Zr^{4+}$ crosslinking agent facilitated the attachment of $Ti_3C_2$ MXenes to the nanogap network electrode. The formation of a DNA–PNA complex in the nanogap network caused a significant change in conductance, which was detected to identify the presence of *M. tuberculosis*. The biosensor demonstrated a limit of detection (LOD) of 20 CFU $mL^{-1}$ and successfully detected the pathogen in 40 simulated sputum samples. The method is rapid, specific, and sensitive, providing a promising approach for *M. tuberculosis* detection.[73]

A recent study by Zhang *et al.*[88] introduces an innovative approach combining MXene materials with CRISPR[89]-Cas12a for the sensitive detection of lipopolysaccharides (LPS) and Gram-negative bacteria. The study highlights how MXene's hydrophilic surface and high density of functional groups allow for efficient adsorption of single-stranded DNA (ssDNA), which enhances target-induced strand release and quenches fluorescence. The method utilizes an aptamer to trigger the *trans*-cleavage activity of CRISPR-Cas12a, resulting in cleavage of ssDNA, leading to fluorescence recovery. This approach demonstrates the potential for selectively quantifying LPS and bacteria in various samples with detection limits of 11 pg $mL^{-1}$ and 23 CFU $mL^{-1}$, respectively. The study offers a novel insight into the application of MXene-based platforms in biosensing and provides a promising pathway for the development of universal analytical methods in microbial detection.[88]

In a study conducted by researchers, a sandwich-like electrochemical immunosensing platform was developed to

 This journal is © The Royal Society of Chemistry 2025

Published on 26 1446. Downloaded on 13/11/47 04:29:14 .

detect Listeria monocytogenes (LM), a common food-borne pathogen. The platform utilized carboxyl $Ti_3C_2T_x$ MXene (C-$Ti_3C_2T_x$ MXene) as the sensing platform and rhodamine B/gold/reduced graphene oxide (RhB/Au/RGO) as a signal amplifier. The high conductivity and large surface area of C-$Ti_3C_2T_x$ MXene enabled the effective immobilization of the primary antibody (PAb) for LM, while the Au/RGO/RhB nanohybrid facilitated the assembly of the secondary antibody (SAb) of LM, enhancing the response signal. The use of rhodamine B as a signal probe enabled the detection of LM, with peak currents increasing as the LM concentration rose from 10 to 105 CFU $mL^{-1}$. The immunosensor achieved an exceptionally low limit of detection (LOD) of 2 CFU $mL^{-1}$ after optimizing experimental conditions. The study concluded that the developed sandwich-like immunosensor based on C-$Ti_3C_2T_x$ MXene and RhB/Au/RGO demonstrated great potential for detecting LM and could be extended to the detection of other pathogens and analytes.[90]

In a study by Guenther *et al.*[91], a label-free electrochemical immunosensor was developed for the effective and rapid detection of *Listeria monocytogenes* in food products. This bacterium is responsible for listeriosis in humans and poses a significant risk to the safety of ready-to-eat food products. The immunosensor was based on a mussel-inspired polydopamine-modified zinc molybdate/MXene (PDA@$ZnMoO_4$/MXene) composite. The sensor exhibited high sensitivity and reliability in detecting *L. monocytogenes* in various food samples, including milk and smoked seafood. Spectrophotometric techniques were employed to assess the properties of the composite materials, while voltammetry and impedimetry were used to confirm the stepwise assembly of the sensor and its detection capabilities. The immunosensor demonstrated a linear detection range from 10 to 107 CFU $ml^{-1}$ and a low detection limit of 12 CFU $ml^{-1}$. It also exhibited excellent selectivity for microbial cocktails and maintained good repeatability, reproducibility, and storage stability. This study suggests that the developed immunosensor, based on PDA surface modification, has promising potential for the detection of *L. monocytogenes* and could be extended to monitor other food-borne pathogens, contributing to enhanced food safety.[91]

A novel electrochemical biosensor targeting bacteriophages has been designed for the accurate and quantitative detection of live *Salmonella* in food samples. The biosensor is constructed by electrostatically immobilizing bacteriophages on MXene-nanostructured electrodes. MXene, known for its high surface area, biocompatibility, and conductivity, serves as an ideal platform for the immobilization of bacteriophages, allowing for a high-density attachment of approximately 71 particles per $\mu m^2$. Remarkably, the bacteriophages immobilized on the MXene nanostructured electrodes maintain their viability and functionality, ensuring their effectiveness in pathogen detection. Consequently, the biosensor demonstrated enhanced sensitivity, with a low limit of detection (LOD) of 5 CFU $mL^{-1}$. Furthermore, the biosensor exhibited excellent specificity in the presence of other bacteria commonly found in food, successfully distinguishing live *Salmonella* from a mixed bacterial population. This biosensor is applicable in detecting live *Salmonella* in food samples, highlighting its potential for food safety monitoring. Its simplicity, convenience, and suitability for resource-limited environments make it a promising tool for on-site monitoring of foodborne pathogenic bacteria.[92]

A study by researchers developed a peptide–target–aptamer sandwich electrochemical biosensor for the detection of Norovirus (NoV), utilizing Au@BP@$Ti_3C_2$-MXene and magnetic Au@$ZnFe_2O_4$@COF nanocomposites. The biosensor's performance was characterized by a detection limit of 0.003 copies per mL, the lowest reported for NoV detection so far. This enhanced sensitivity is attributed to the specific recognition capabilities of the aptamer and affinity peptide, combined with the outstanding catalytic properties of the nanocomposites. The sensor demonstrated remarkable selectivity, anti-interference properties, and stability. Successful detection of NoV was achieved in both simulated food matrices and stool samples without requiring complex pretreatment. The biosensor's performance indicates significant potential for detecting NoV in food, clinical, and environmental samples, offering a new approach to foodborne pathogen detection[63] (Fig. 1D).

A study conducted by other researchers developed an interference-free surface-enhanced Raman scattering (SERS) platform for the detection of extended-spectrum β-lactamase (ESBL) producing *E. coli* (ESBL-*E. coli*). In this work, 4-mercaptomethylboronic acid (4-MPBA) was used as a capture molecule for drug-resistant bacteria, and self-assembled gold nanoparticles (Au NPs) were employed to develop a high-performance SERS platform. The research further utilized $Ti_3C_2T_x$, modified with 4-mercaptobenzonitrile (4-MBN) and Au NPs, to enhance the signal and enable indirect detection. The SERS platform demonstrated the capability to detect signals from the Raman silent region, where no background signal from biological sources interfered. This feature eliminated interference, allowing for highly sensitive detection with a limit of detection as low as 10 CFU $mL^{-1}$, and a wide dynamic linear range from $10–10^8$ CFU $mL^{-1}$. The stability, homogeneity, and reproducibility of the platform were excellent, and the detection capability was validated through the identification of ESBL-*E. coli* in milk samples. This work highlights the promising potential of the SERS platform for the stable and sensitive detection of drug-resistant bacteria, contributing to the advancement of antimicrobial detection technologies.[93]

### 3.3. MXene-based sensors in viral detection

MXenes, a class of 2D materials, have emerged as promising candidates for use in antimicrobial applications. These materials, including $Ti_3C_2T_x$, $Ta_4C_3T_x$, and $Nb_2CT_x$, possess hydrophilic surfaces and high negative charges, which make them effective for use as coatings on facemasks for virus capture and inactivation.[94] Their high surface area and porosity enable strong adsorption of amino acids and viral spike proteins, thereby immobilizing viruses. Additionally, MXenes exhibit photocatalytic properties, meaning that viruses

Published on 26 1446. Downloaded on 13/11/47 04:29:14 .

adsorbed on their surface can be destroyed when exposed to light. For instance, $Ti_3C_2T_x$ MXene can be excited by red light (at 780 nm plasmon resonance), and this energy can be used for virus sterilization, either with infrared lamps or solar light.[95] Furthermore, MXenes possess antibacterial characteristics due to their charge transfer properties and hydrophilicity. As a widely used, low-cost material, titanium carbide MXenes do not have harmful environmental or toxicological effects, making them safe for biomedical applications. These features position MXenes as highly effective materials for addressing challenges in pathogen detection and antimicrobial treatments, with applications in various medical devices.[96]

MXenes have also been explored for their potential in medical settings beyond pathogen detection. For instance, they have been shown to be capable of regenerating dialysate by removing toxins that accumulate in cases of kidney failure, offering an efficient solution for patients undergoing hemodialysis. This ability stems from the slit pores between the negatively charged MXene sheets, which facilitate the absorption of urea, a common waste product that is difficult to eliminate through traditional dialysis. Given their biocompatibility, small size, and lightweight properties, MXenes offer a promising alternative to current dialysis systems.[97]

In a study by Uzunoglu *et al.*[98], a novel approach was presented for the development of MXene-based sensors for the detection of SARS-CoV-2. The research highlights the potential of $Ti_3C_2T_x$ MXenes in biosensing applications, owing to their high surface area, electrical conductivity, and hydrophilicity. These properties make MXenes ideal for use in functional electrodes designed for the detection of viral pathogens, particularly SARS-CoV-2. The $Ti_3C_2T_x$ MXenes were functionalized with probe DNA molecules through noncovalent adsorption, which eliminated the need for expensive labeling techniques while ensuring sequence-specific recognition of the target gene. This method facilitated the detection of the nucleocapsid (N) gene of SARS-CoV-2 through nucleic acid hybridization and chemoresistive transduction. The developed sensors demonstrated sensitive and selective detection, achieving a detection limit below 105 copies per mL in saliva samples. The sensors also showed high specificity when tested against related coronaviruses, such as SARS-CoV-1 and MERS. The interlayer spacing of MXenes was hypothesized to serve as molecular sieving channels, enhancing their capability to host organic molecules and ions. This characteristic is considered a significant advantage in the context of biomolecular sensing and suggests that MXene-based sensors may offer an effective, cost-efficient solution for point-of-care detection of viral pathogens.[98]

In a recent study, $Ti_3C_2$ MQDs were synthesized and their potential for mitigating SARS-CoV-2 infection was investigated. The MQDs were characterized using various physicochemical methods, revealing the presence of bioactive functional groups such as oxygen, hydrogen, fluorine, and chlorine, as well as surface titanium oxides. The efficacy of MQDs was tested in VeroE6 cells infected with SARS-CoV-2. The results demonstrated that the treatment with MQDs significantly reduced the multiplication of virus particles at very low doses (0.15 μg $mL^{-1}$). To further understand the mechanisms underlying the anti-viral properties of MQDs, global proteomics analysis was performed, identifying differentially expressed proteins between MQD-treated and untreated cells. The findings indicated that MQDs interfere with the viral lifecycle through multiple mechanisms, including modulation of the $Ca^{2+}$ signaling pathway, IFN-α response, virus internalization, replication, and translation. These findings suggest that MQDs hold promise as a nanotherapeutic candidate for developing future immunoengineering-based strategies against SARS-CoV-2 and other viral infections.[99]

In a study by Jiang *et al.*[100], a novel approach was developed for rapid viral detection using MXene-based sensors. Traditional monoclonal antibody-based immunoassays face challenges such as high costs, fragility, and instability, particularly in complex media. To address these issues, the researchers engineered dual-epitope nanobodies (NBs), which were incorporated into a sandwich immunosensor design for detecting rotavirus antigens in samples like rectal swabs and wastewater. To further enhance the sensor's performance, MXenes@CNTs@AuNPs (MXene, carbon nanotubes, and gold nanoparticles) were synthesized. This composite provided a large specific surface area that facilitated the enrichment and immobilization of NBs, allowing for efficient signal generation when combined with catalase-modified magnetic probes. The resulting sensor achieved an impressive detection limit of 0.0207 pg $mL^{-1}$ for the rotavirus VP6 antigen, showing a $3.77 \times 10^5$ fold increase in sensitivity compared to commercial antigen kits. The sensor demonstrated exceptional performance in terms of specificity, repeatability, stability, and accuracy across various sample types, positioning it as a promising tool for rotavirus detection. This research outlines a robust strategy for developing ultrasensitive viral detection tools, addressing the need for efficient and reliable methods in diverse environments.[100]

The ongoing evolution of influenza viruses is critical for the seasonal outbreaks and occasional pandemics affecting humans. Among the different types of influenza (A, B, C, and D), type A is primarily responsible for seasonal spread. Influenza A viruses are further classified based on surface proteins, hemagglutinin (HA) and neuraminidase (NA). In the last decade, frequent outbreaks of HA subtypes have occurred globally, including strains such as H1N1, H2N2, H3N2, H5N1, and H7N1, among others. These outbreaks have raised concerns regarding the spread of the virus and the need for efficient detection methods to monitor and control its transmission. The detection and monitoring of influenza, as well as other viral pathogens, are crucial in preventing widespread infections. The use of MXene-based biosensors has been explored as a promising approach to detect viruses like influenza with high sensitivity. The inherent properties of MXenes, such as large surface area, good electrical conductivity, and biocompatibility, make them suitable for the development of highly efficient sensors capable of detecting viral particles, including

 This journal is © The Royal Society of Chemistry 2025

Published on 26 1446. Downloaded on 13/11/47 04:29:14 .

influenza viruses. Such sensors are poised to play a significant role in early detection, potentially improving response times to viral outbreaks.[101]

A study conducted by Li *et al.*[68] developed a MXene-graphene field-effect transistor (FET) biosensor for influenza virus sensing. This biosensor leverages the high chemical sensitivity of MXenes combined with the large-area, high-quality graphene to create an ultra-sensitive virus-sensing transduction material (VSTM). Previous research had demonstrated the use of graphene FET sensors for influenza detection; however, these devices exhibited limitations such as a relatively low signal-to-noise ratio, which reduced their robustness and required virus sample pre-processing. To address these challenges, the team incorporated MXenes into the graphene-based FET biosensor, enhancing the sensitivity and performance of the device. The developed MXene-graphene composite sensor demonstrated a low detection limit (125 copies per mL) for inactivated influenza A (H1N1) HA virus antigens and an average response time of approximately 50 ms, significantly outperforming existing real-time reverse transcription-polymerase chain reaction (RT-PCR) methods, which typically take over 3 hours. Additionally, the sensor was successfully applied to detect 2019-nCoV spike proteins, showing a linear detection range from 1 fg $mL^{-1}$ to 10 pg $mL^{-1}$ and a detection limit of 1 fg $mL^{-1}$ for the recombinant protein, with results available in 50 ms. This advancement highlights the potential of MXene-based sensors for rapid, accurate, and cost-effective viral detection, positioning them as a promising alternative to conventional methods like RT-PCR and rapid influenza diagnostic tests (RIDTs).[102]

In a study conducted by researchers, a colorimetric and fluorescent dual-functional two-channel immunochromatographic assay (ICA) biosensor was developed for the simultaneous detection of influenza A virus (FluA) and SARS-CoV-2. This biosensor utilized a unique two-dimensional $Ti_3C_2$ quantum dot (QD) immunoprobe, which involved adsorbing dense QDs onto the light green monostromatic $Ti_3C_2$ MXene surface. This design resulted in light green colorimetric signals and enhanced fluorescence, ensuring high sensitivity, stability, and excellent liquidity for ICA detection. The biosensor allowed for rapid visual screening of FluA and SARS-CoV-2 through the green colorimetric signal, as well as sensitive and quantitative detection of the viruses in the early stages of infection through fluorescence. The proposed $Ti_3C_2$-QD-ICA biosensor demonstrated excellent sensitivity and accuracy, achieving detection limits of 1 ng $mL^{-1}$ for FluA and 1 ng $mL^{-1}$ for SARS-CoV-2 in colorimetric and fluorescence modes, respectively. This method offered faster results and better reproducibility compared to conventional gold nanoparticle (AuNP)-based ICA methods, with a testing time of only 20 minutes. The results suggest that this $Ti_3C_2$-QD-ICA method could be applied for the rapid, ultrasensitive, and multiplex detection of respiratory viruses, showing promise in virology diagnostics[64] (Fig. 1E).

A label-free surface plasmon resonance (SPR) aptasensor has been developed for the detection of the N-gene of SARS-CoV-2 using thiol-modified niobium carbide ($Nb_2C$-SH) QDs as the bioplatform for anchoring the N-gene-targeted aptamer. In the presence of SARS-CoV-2 N-gene, the immobilized aptamer strands undergo conformational changes that specifically bind with the N-gene, resulting in either an increased contact area or an enlarged distance between the aptamer and the SPR chip. This leads to a change in the SPR signal, which is measured by a laser (He–Ne) at a wavelength of 633 nm. The $Nb_2C$-SH QDs, derived from $Nb_2C$ MXene nanosheets through a solvothermal method and functionalized with octadecanethiol, were used to modify the SPR chip *via* covalent binding. The sensor demonstrated a low limit of detection (LOD) of 4.9 pg $mL^{-1}$ for the N-gene, with a concentration range of 0.05 to 100 ng $mL^{-1}$. Additionally, the sensor exhibited excellent selectivity for the N-gene in the presence of various respiratory viruses and proteins in human serum and demonstrated high stability. The $Nb_2C$-SH QD-based SPR aptasensor was successfully applied for the qualitative analysis of the N-gene in various sample types, including seawater, seafood, and human serum. This work provides a comprehensive understanding of the construction of aptasensors for viral detection in complex environments and highlights the potential of MXene-based sensors in virology[65] (Fig. 1F).

In a study conducted by researchers, a collaborative detection system was developed that integrates high-load hybridization probes targeting the N and ORF1a genes of SARS-CoV-2 with Au NPs@$Ta_2C$-M-modified gold-coated tilted fiber Bragg grating (TFBG) sensors. This system enables the direct nucleic acid detection of the virus. The researchers used a segmental modification approach, where multiple activation sites of SARS-CoV-2 were modified on the surface of a homogeneous array of AuNPs@$Ta_2C$-M/Au structures. The combination of hybrid probe synergy and composite polarization response resulted in highly specific hybridization analysis and excellent signal transduction for trace target sequences. This platform exhibited a detection limit of 0.2 pg $mL^{-1}$ and a rapid response time of 1.5 minutes for clinical samples without the need for amplification. The results demonstrated high agreement with the traditional RT-PCR test (Kappa index = 1). This study suggests that the proposed detection system has the potential to support the global effort to curb epidemics like COVID-19 by offering a rapid and accurate diagnostic tool.[103]

In response to the COVID-19 pandemic, there has been significant advancement in Point-of-Care Testing (POCT) devices for the detection of SARS-CoV-2. A study by Chen *et al.*[104] demonstrated the development of a DNA primer-functionalized $Ti_3C_2T_x$ MXene-based biosensor designed for the rapid and accurate detection of the SARS-CoV-2 nucleocapsid (N) gene. This biosensor exhibits high selectivity and sensitivity, with the sensor response increasing in proportion to the amount of target DNA added. The SARS-CoV-2 N gene was detected after heat inactivation at 65 °C for 30 minutes. The inactivated virus sample was identified using ssDNA/$Ti_3C_2T_x$ sensors, with validation conducted through one-step qRT-PCR and agar gel electrophoresis. A clear band corresponding to a 72 base-pair length was observed, which aligns with prior PCR

Published on 26 1446. Downloaded on 13/11/47 04:29:14 .

findings. The sensor's ability to detect varying concentrations of the heat-inactivated SARS-CoV-2 N gene was evaluated, with real-time detection capabilities confirmed through differential responses in sensor current as target gene concentrations increased. The biosensor demonstrated a low detection limit of fewer than 105 copies per mL, with a nearly linear response across a broad concentration range from 105 to 109 copies per mL. This makes the sensor highly effective for detecting viral loads, particularly during the early stages of infection, when patients typically exhibit symptoms. While slightly less sensitive when tested with saliva compared to buffer, the device showed minimal fluctuation between devices. The findings highlight the significant potential of MXene-based biosensors in viral detection, particularly for rapid and sensitive identification of SARS-CoV-2, which could contribute to more effective monitoring and control of the virus during its early stages [66,104](Fig. 1G).

A study was conducted to develop a highly sensitive electrochemical luminescence (ECL) biosensor for the detection of HIV-1 protein, using $Ti_3C_2T_x$-modified ZIF-8 as an ECL emitter. The sensor was designed to detect HIV-1 with high sensitivity, utilizing 0.05 M $K_2S_2O_8$ as the co-reactant and conductive carbon black combined with magnetic nanoparticles as the quenching agent. The sensor showed a linear response within the concentration range of 1 fM to 1 nM, with a detection limit of 0.3 fM (S/N = 3), demonstrating its potential for early detection of HIV. Additionally, when applied to real serum samples, the sensor displayed great recoveries, highlighting its practical application for HIV-1 detection. This study emphasizes the effectiveness of MXene-based biosensors in viral detection, showcasing their potential for improving diagnostic accuracy and sensitivity in clinical settings. The research demonstrates the promising role of MXenes in the development of advanced biosensors for detecting viral infections, supporting their broader application in microbiology and virology.[71]

A study by Wang *et al.*[71] introduced a novel ECL biosensor for the detection of HIV-1 protein using a combination of metal–organic frameworks (ZIF-8) and $Ti_3C_2T_x$ MXene as an ECL emitter. The $Ti_3C_2T_x$ nanomaterial was modified through etching with HF, and ZIF-8 was incorporated to enhance the conductivity and stability of the nanocomposite. The fabricated biosensor exhibited excellent sensitivity with a low detection limit of 0.3 fM and remarkable selectivity for HIV-1 protein. The detection was successfully carried out in real serum samples, with recoveries ranging from 86.0% to 115.8%, demonstrating the practical application of this biosensor for detecting HIV-1 in complex biological samples.

The integration of polyacrylic acid (PAA) further prevented agglomeration between $Ti_3C_2T_x$ layers and facilitated better interaction with ZIF-8. This ECL biosensor demonstrated high sensitivity, with a detection limit as low as 0.3 fM and excellent selectivity for HIV-1 protein. When tested with serum samples, the biosensor showed recoveries ranging from 86.0% to 115.8%, confirming its potential for practical applications in HIV-1 detection.[71] A study by Peng *et al.*[26] explored the use of MXene $Ti_3C_2$ nanosheets as a sensing platform for the selective detection of Human Papillomavirus (HPV). These MXene nanosheets demonstrated high fluorescence quenching ability when interacting with dye-labeled single-stranded DNA (ssDNA) and exhibited strong affinity for both ssDNA and double-stranded DNA (dsDNA). The fluorescent biosensor they developed for the detection of HPV-18 displayed high specificity and a low detection limit of 100 pM. However, it was noted that fluorescent biosensors face challenges such as ineffective signal transduction and a lack of wireless data transmission capabilities, limiting their use as smart sensors due to the difficulty in balancing sensitivity and portability. To address these limitations, Zeng *et al.*[105] developed a CRISPR-Cas12a-based piezo-resistive biosensor integrating MXene $Ti_3C_2T_x$-PEDOT:PSS/PDMS. This system provided high sensitivity and portability, allowing for real-time wireless transmission of nucleic acid detection signals. The system combined CRISPR-Cas12a-mediated target-activated gas-producing reactions with flexible MXene-modified electrodes, enabling continuous, real-time HPV-related DNA detection. Experimental and theoretical simulations confirmed that this biosensor exhibited excellent force-to-electric conversion capabilities and demonstrated good reproducibility and accuracy.[105]

## 4. Antimicrobial and antiviral properties of MXenes

It has been reported that infections caused by pathogenic bacteria present significant threats to public health. Traditional bacterial detection and treatment methods often encounter limitations related to sensitivity and antibiotic resistance. In prior research, the synthesis methods and structural characteristics of MXenes were comprehensively investigated, encompassing both top-down and bottom-up approaches. Additionally, efforts were directed toward developing bacterial detection sensors. Studies have demonstrated the effectiveness of MXene-based electrochemical, fluorescent, and dual-modal sensors in enhancing sensitivity and precision in detecting bacteria, with a particular emphasis on the capability of MXenes to identify chiral molecules. Furthermore, antibacterial mechanisms mediated by MXenes were explored, including physical disruption, photothermal sterilization, and reactive oxygen species (ROS)-driven bacterial eradication. Applications in water purification and antibacterial treatments were also discussed, highlighting their practical utility. The potential for future advancements in MXene-based bacterial detection and antibacterial applications was emphasized, offering a comprehensive overview of progress in this area.[106]

The increasing prevalence of bacterial infections and the growing resistance to available antibiotics pose significant threats to human health and the environment. While antibiotics are crucial in combating bacterial infections, their overuse weakens the immune system and contributes to the development of antibiotic resistance. These issues have led to

 This journal is © The Royal Society of Chemistry 2025

Published on 26 1446. Downloaded on 13/11/47 04:29:14 .

concerns about the clinical use of antibiotics. In response, there is a pressing need to explore alternative antibacterial strategies. MXenes, a class of two-dimensional materials, have gained attention for their promising applications in tumor therapy and biosensing due to their unique properties, such as a large specific surface area, high chemical stability, hydrophilicity, wide interlayer spacing, and excellent adsorption and reduction capabilities. These characteristics suggest MXenes could be valuable for biopharmaceutical applications. However, research on their antimicrobial properties remains limited. Current antimicrobial mechanisms of MXenes include physical damage to bacterial membranes, oxidative stress induction, and the use of photothermal and photodynamic therapies. Recent studies have explored these mechanisms, which highlight the potential of MXenes in addressing bacterial infections. The mechanisms are primarily attributed to:[107] physical damage to bacterial membranes due to the sharp edges of the material,[108] chemical damage caused by oxidative stress, and[109] the enhancement of antimicrobial effects through near-infrared phototherapy.[6]

Researchers have investigated how MXene composite materials function as antibacterial agents. The primary antibacterial mechanisms have been categorized into NanoKnives, ROS (Reactive Oxygen Species) Generators, and Nanothermal Blades. In this study, it has been reported that the sharp edges of MXene nanosheets damage bacterial cells, facilitating the endocytosis of gold nanoclusters (AuNCs), which then generate ROS to cause oxidative damage to the bacterial cell membrane and DNA. This dual-action mechanism is effective against both Gram-positive and Gram-negative bacteria. The antibacterial efficacy of MXenes, particularly thinner ones like $Nb_2CT_x$, has been shown to be more effective against microorganisms such as *Staphylococcus aureus*, *Bacillus subtilis*, *E. faecalis*, *Klebsiella pneumoniae*, and *Escherichia coli* (Table 2). The sharp edges of these thinner MXenes effectively cut bacterial membranes, while their ROS-generating properties further contribute to the destruction of microbial cells. MXene-based composite materials also demonstrate versatility for various healthcare applications, such as wound dressings, anti-biofouling membranes, solar-driven water purification, food packaging, and textiles. MXenes are powerful materials with potential for antibacterial therapeutic applications. However, further research is needed to fully understand their antibacterial mechanisms. A deeper exploration of how these two-dimensional nanomaterials interact with microbes will enable the development of more effective treatment methods in the future. It is crucial to continue theoretical and applied research to expand the applicability of MXene-based antibacterial materials across a broader range of fields.[110]

In a study investigating the antibacterial properties of $Ti_3C_2T_x$ MXene, it was demonstrated that single- and few-layer $Ti_3C_2T_x$ MXene flakes possess significant antibacterial activity against both Gram-negative *Escherichia coli* (*E. coli*) and Gram-positive *Bacillus subtilis* (*B. subtilis*) in colloidal solutions (Table 2). The antibacterial efficiency of $Ti_3C_2T_x$ was evaluated by bacterial growth curves based on optical densities and colony counts on agar plates. The results showed that $Ti_3C_2T_x$ exhibited higher antibacterial effectiveness compared to graphene oxide (GO), a widely reported antibacterial agent. Concentration-dependent antibacterial activity was observed, with over 98% bacterial cell viability loss at 200 μg $mL^{-1}$ of $Ti_3C_2T_x$ within 4 hours of exposure. This was further confirmed by colony forming unit (CFU) assays and regrowth curves.

The underlying antibacterial mechanism was investigated using scanning electron microscopy (SEM) and transmission electron microscopy (TEM), alongside lactate dehydrogenase (LDH) release assays, revealing significant damage to bacterial cell membranes and the release of cytoplasmic materials. The study also examined the induction of reactive oxygen species (ROS)-dependent and independent stress by $Ti_3C_2T_x$ through separate abiotic assays. These findings indicate that $Ti_3C_2T_x$ MXene flakes show promising potential for antibacterial applications, including resistance to biofouling, and can be considered for use in a range of antimicrobial applications, particularly in water filtration and biomedical devices.[111]

MXenes represent a novel class of materials that have been demonstrated to possess effective mechanisms against bacteria. Researchers have explored multiple antibacterial mechanisms of MXene composite materials, categorizing them into NanoKnives, ROS Generators, and Nanothermal Knives. The sharp edges of MXene nanosheets can physically disrupt bacterial cells, facilitating the uptake of AuNCs and triggering DNA oxidation. This process leads to the production of reactive oxygen species (ROS), which compromise the bacterial cell membrane and contribute to the elimination of both Gram-positive and Gram-negative bacteria. Despite these promising effects, the antimicrobial properties of MXenes remain an emerging area of study, necessitating further research to clarify their mechanisms and overall impact (Fig. 2A).[110]

• MXenes as NanoKnives: initial studies suggest that MXenes, a class of 2D nanosheets, possess antibacterial properties similar to those of graphene oxide (GO). Their antibacterial action primarily involves the physical disruption of bacterial cell membranes. The sharp edges of MXene nanosheets, often referred to as "nano-knives", play a key role in damaging bacterial cell walls, leading to membrane rupture and cytoplasmic leakage. Higher concentrations of MXenes have been observed to form thin layers that envelop bacterial cells and aggregate into larger structures. Beyond their sharp edges, additional factors contribute to their antimicrobial activity. The hydrophilic and negatively charged nature of MXenes interferes with bacterial nutrient uptake by interacting with lipopolysaccharides on the cell surface. Additionally, MXenes enhance their bactericidal effects through hydrogen bonding, further compromising bacterial integrity.[117] Extending the exposure time to eight hours enhances MXene's antimicrobial effectiveness to over 95%. Its antibacterial action begins when the nanosheets come into direct contact with the bacterial surface. The sharp edges of MXene play a crucial role in piercing and disrupting the bacterial cell membrane, which ranges from 20 to 50 nm in thickness. Smaller MXene nanosheets can

Published on 26 1446. Downloaded on 13/11/47 04:29:14 .

**Table 2** A schematic representation of MXene structures utilized as antibacterial agents against various bacterial species, along with the methods employed for susceptibility assessment

| Type of MXene | Type of bacteria | Susceptibility method | Ref. |
|---|---|---|---|
| $Ti_3C_2T_X$ 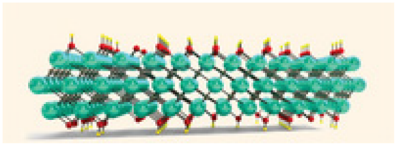 | • *Escherichia coli*<br>• *Bacillus subtilis* | • Plate colony count<br>• Flow cytometry<br>• Fluorescence Imaging | 112 and 113 |
| $Ti_2CT_X$ 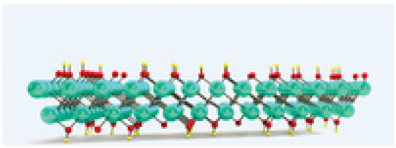 | • *Staphylococcus aureus*<br>• *Bacillus subtilis*<br>• *Sarcina* | • Disk diffusion | 112 and 114 |
| $V_2CT_X$+NIR 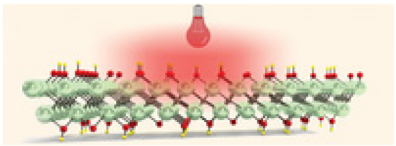 | • *Escherichia coli*<br>• *Staphylococcus aureus*<br>• *Bacillus subtilis* | • Plate colony count<br>• Disk diffusion | 112 |
| $Nb_2CT_X$+NIR 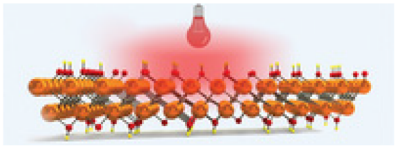 | • *Pseudomonas aeruginosa*<br>• *Acinetobacter baumannii*<br>• *Salmonella typhi*<br>• *Burkholderia cepacia*<br>• *Enterobacter cloacae*<br>• *Klebsiella aerogenes*<br>• *Proteus mirabilis*<br>• *VRE*<br>• *Enterococcus faecalis*<br>• *Streptococcus agalactiae*<br>• *Klebsiella pneumoniae* | | |
| $Ti_3C_2T_X$+NIR 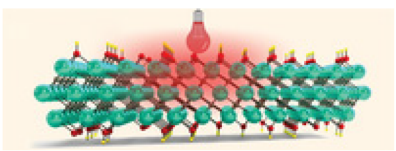 | | | 112 and 115 |

enter bacterial cells through endocytosis or physical penetration. Once inside, these nanosheets intensify their bactericidal effect by breaking down bacterial DNA, further contributing to cell destruction (Fig. 2B).[110]

• MXenes as ROS generators: reactive oxygen species (ROS) are oxygen molecules with unpaired electrons, known for their ability to eliminate microorganisms and cancer cells.[118] MXenes, when combined with ultrasound, have been widely explored in cancer treatment due to their ROS-generating capabilities. However, their response to ultrasound in antibacterial applications remains largely unexplored. Many 2D nanomaterials are recognized for inducing oxidative stress through ROS production, and MXenes are believed to exert antibacterial effects through similar mechanisms influenced by their electrical properties. The formation of ROS in MXenes is closely linked to their structural and electrical characteristics, which are influenced by factors such as the number of MXene layers, stacking arrangement, size, defects, and doping. Understanding these variables is essential for optimizing the antibacterial potential of MXenes.[119]

• MXenes as Nanothermal blades: MXene has been shown to possess bactericidal properties through photothermal mechanisms. Its molecular structure plays a key role in damaging bacterial cell membranes. The heat generated by MXene directly affects the bacterial membrane, disrupting intracellular homeostasis and increasing membrane permeability. This thermal effect also leads to the denaturation of proteins and DNA.[120]


This journal is © The Royal Society of Chemistry 2025

Published on 26 1446. Downloaded on 13/11/47 04:29:14 .

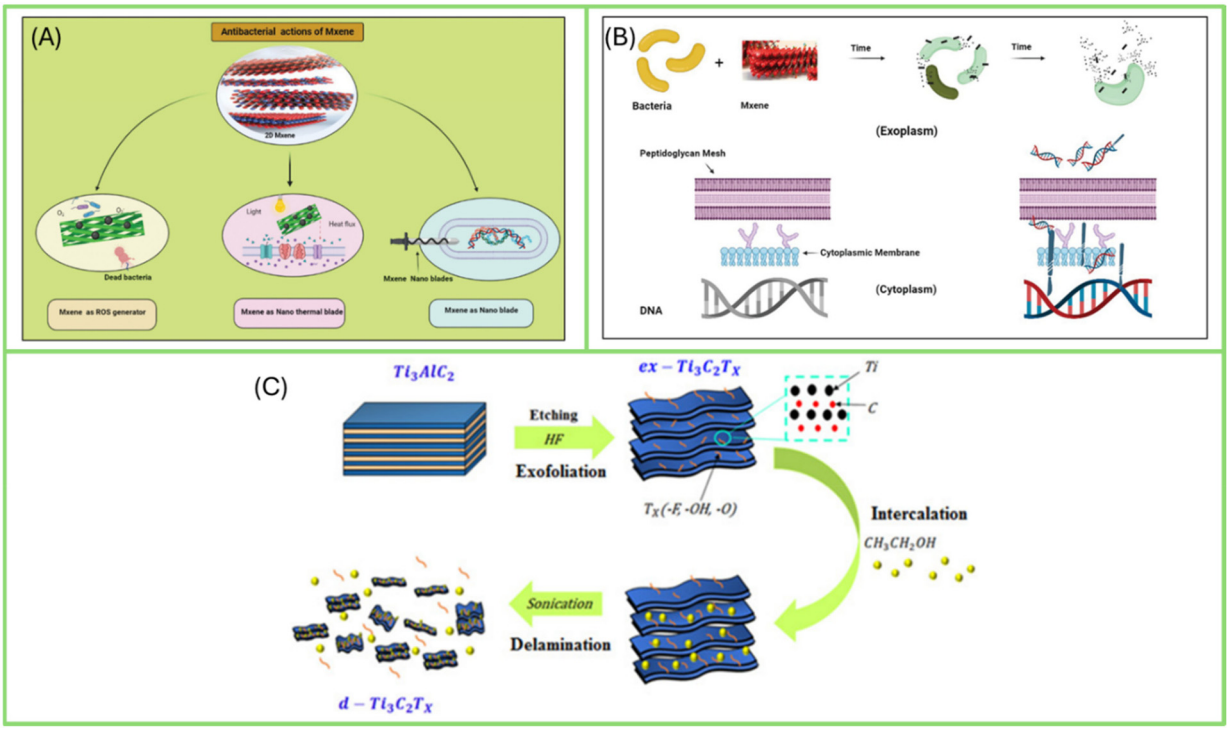


**Fig. 2** (A) Schematic summary provides an overview of the antibacterial mechanism of action of MXene against various microorganisms.[110] Copyright 2023 American Chemical Society. (B) Schematic summary illustrates the antimicrobial mechanism of $Ti_3C_2T_x$ nanosheets.[110] Copyright 2023 American Chemical Society. (C) Schematic summary demonstrates that $Ti_3C_2T_x$ MXene nanosheets exhibit an antifungal effect by suppressing the hyphal growth of Trichoderma reesei fungus.[116] Copyright 2020 Elsevier.

The combined action of heat and sharp edges gives MXene a "nano-thermal knife" effect, enabling efficient bacterial destruction.[121] However, the hydrophilic nature of $Ti_3C_2T_x$ does not inherently promote penetration through the hydrophobic lipid layers of bacterial membranes. The energy barrier for penetration is influenced by the direction and angle of interaction. Molecular dynamics simulations are valuable tools for gaining deeper insights into the bactericidal mechanisms of MXene.

While MXenes has attracted attention with its activity against bacteria in recent years, it is thought that it may exhibit potential antifungal properties against fungi. In this study, the antifungal properties of $Ti_3C_2T_x$ MXene nanosheets were explored for the first time, although their antibacterial properties are already well-established. $Ti_3C_2T_x$ MXene was synthesized by stripping the $Ti_3AlC_2$ MAX phase with hydrofluoric acid, followed by intercalation and delamination using ethanol treatment and ultrasonication. The delaminated $Ti_3C_2T_x$ MXene nanosheets (d-$Ti_3C_2T_x$) were characterized using various techniques, revealing a lamellar structure with alternating layers of Ti, Al, and C. X-ray diffraction (XRD) and Raman spectroscopy confirmed the removal of Al and the formation of two-dimensional $Ti_3C_2T_x$ MXene nanosheets. Antifungal activity was assessed using the modified agar disc method against Trichoderma reesei. Observations under inverted phase contrast microscopy showed a significant inhibition of hyphal growth around the MXene-treated discs, with abundant hyphal and spore formation observed only in the control group. Additionally, fungal spores treated with d-$Ti_3C_2T_x$ MXene nanosheets failed to germinate even after 11 days. These results indicated disruption of the fungal colony's hemispherical structure, inhibition of hyphal growth, and cell damage. Therefore, the findings suggest that the developed d-$Ti_3C_2T_x$ MXene nanosheets have promising potential as antifungal agents[116] (Fig. 2C).

### 4.1. Antimicrobial mechanisms of MXenes: bacterial membrane disruption

Recent studies have highlighted the growing concern of antimicrobial resistance exhibited by viruses, bacteria, and fungi, prompting the need for the development of new materials with high efficacy.[122] MXenes have shown significant bactericidal effects, inhibiting the growth of both Gram-positive and Gram-negative bacteria by disrupting their cell membranes. Additionally, MXenes have been found to possess antifungal properties, showing potential for addressing fungal infections. Emerging research also suggests that certain MXenes exhibit antiviral activity, impacting both enveloped and non-enveloped viruses. These materials are being explored for applications in wound healing, where they prevent infections and accelerate the healing process. Furthermore, MXenes are being integrated into various materials, including coatings, composites, and surfaces for use in medical devices, textiles, and food packaging to provide antimicrobial protection. The potential of

Published on 26 1446. Downloaded on 13/11/47 04:29:14 .

MXenes in photothermal and photodynamic therapy has also been recognized, as they can target and eliminate cancer cells or pathogens when activated by light. While the biocompatibility and toxicity of MXenes remain critical considerations, ongoing research aims to overcome these challenges and explore their broader application in combating antimicrobial resistance. MXenes hold considerable promise for advancing medical technologies and addressing the global threat posed by antimicrobial resistance. This study introduces a broader understanding of MXenes by highlighting their antiviral and antifungal properties, which were less emphasized in earlier studies. It also expands on their applications in medical devices, wound healing, and advanced therapies like photothermal treatment, offering new perspectives on their potential. Additionally, the review addresses biocompatibility and toxicity concerns, providing a comprehensive view of MXenes' role in combating antimicrobial resistance and advancing medical technologies[123] (Fig. 3A).

The antibacterial mechanism of two-dimensional (2D) nanomaterials, including MXenes, primarily involves the mechanical disruption of bacterial membranes due to the sharp edges or rough surfaces of the materials. The antibacterial properties of $Ti_3C_2T_x$ MXene were first investigated by Rasool *et al.*,[129] who observed membrane integrity and bacterial morphology changes following interaction with *E. coli* and *B. subtilis*. Scanning electron microscopy (SEM) and transmission electron microscopy (TEM) revealed that, in the control group, the bacterial membranes remained intact, while, in the experimental group, severe membrane damage and cytoplasmic leakage were evident. The degree of bacterial damage increased with $Ti_3C_2T_x$ concentration, resulting in complete cell lysis and rupture of the bacterial membrane at 100 μg $mL^{-1}$. TEM images further showed that $Ti_3C_2T_x$ nanosheets adsorbed strongly around the bacterial cells and even penetrated them, leading to a reduction in intracellular density, indicating the loss of cytoplasmic material. Pandey *et al.*[130] studied $Nb_2C_2T_x$ and $Nb_4C_3T_x$ nanosheets and observed that these nanosheets were absorbed by the cell walls of *S. aureus* and *E. coli*. Some nanosheets entered the bacterial cells, forming pores and disrupting the cell wall and cytoplasmic membrane. This process led to the efflux of cellular contents, cell deformation, and significant damage to intracellular structures. Further work by Arabi Shamsabadi *et al.*[131] on the growth of *B. subtilis* and *E. coli* strains induced by $Ti_3C_2T_x$ nanosheets of varying sizes showed that the sharp edges of the nanosheets physically interacted with the bacterial membrane, causing membrane damage and the release of cytoplasmic DNA. The antimicrobial effect was found to depend on the size of the nanosheets, with smaller nanosheets being more capable of penetrating the bacteria and disrupting cytoplasmic components *via* physical penetration or endocytosis, as supported by findings from both Rasool *et al.*[124] and Pandey *et al.*[130] The LDH release assay conducted by Rasool *et al.*[129] demonstrated a dose-dependent increase in the release of LDH with increasing concentrations of $Ti_3C_2T_x$, indicating that both the bacterial cell wall and contents were damaged. These results suggest that the sharp edges of MXenes are one of the primary mechanisms by which they exert antimicrobial effects, leading to significant physical damage to bacterial membranes[124,125] (Fig. 3B).

Previous studies have demonstrated that oxidative stress plays a key role in the bactericidal effects of various nanomaterials, including metal, metal oxide, and carbon-based materials. MXenes induce oxidative stress through the generation of reactive oxygen species (ROS) such as singlet oxygen ($1O_2$), hydroxyl radicals (OH), superoxide anion ($O^{2-}$) and hydrogen peroxide ($H_2O_2$). These ROS contribute to the damage of essential cellular components, including proteins, lipids, DNA, and RNA.[132] MXenes typically exhibit a negative zeta potential, which enhances their affinity for cell surfaces, facilitating interactions that can lead to the generation of ROS. The high conductivity of MXenes also allows them to transfer electrons effectively, further promoting ROS production through interactions with the lipid bilayers of bacterial cells. Pandey *et al.*[130] explored the antimicrobial mechanism of MXenes such as $Nb_2CT_x$ and $Nb_4C_3T_x$, using glutathione (GSH) oxidation to assess oxidative stress. Their findings indicated that both materials caused GSH depletion, but $Nb_4C_3T_x$ exhibited a stronger oxidative effect, which may be attributed to its larger interlayer spacing and enhanced charge transfer activity compared to $Nb_2CT_x$. Zheng *et al.*[133] investigated the antibacterial potential of MXenes and reported that ROS production by MXene was 1.8 times higher than the control group, with subsequent lipid peroxidation assays showing that MXene induced oxidative damage to bacterial membranes. This indicates the ability of MXenes to cause oxidative stress and damage bacterial structures. However, they did not identify which specific ROS were responsible for this activity. Rasool *et al.*[129] also examined the oxidative potential of $Ti_3C_2T_x$ MXene by monitoring superoxide anion ($O^{2-}$) production through the XTT method, though no significant contribution was found from $O^{2-}$ to the antimicrobial effect. This suggests that additional ROS species (such as OH, $1O_2$, and $H_2O_2$) may play a more significant role in MXene-induced antimicrobial activity.

The antimicrobial properties of MXenes, particularly in combating antibiotic-resistant bacteria such as methicillin-resistant *Staphylococcus aureus* (MRSA), have garnered significant interest in recent years. A study by Ezraty *et al.*[134] and Zou *et al.*[135] introduced Near-Infrared Light (NIRL) therapies, specifically photodynamic therapy (PDT) and photothermal therapy (PTT), as promising strategies to enhance the antimicrobial efficacy of MXenes against resistant bacteria. PTT utilizes photothermal agents (PTAs) to convert light energy into heat, causing bacterial membrane rupture and irreversible damage. PDT, on the other hand, employs photosensitizers (PS) to generate reactive oxygen species (ROS) under light exposure, which disrupt bacterial membranes and lead to cell death. MXenes, particularly $Ti_3C_2T_x$ nanosheets, have demonstrated exceptional light absorption properties in the near-infrared (NIR) region, making them highly effective for these therapies. The MXene-based materials exhibit both photother-

 This journal is © The Royal Society of Chemistry 2025

Published on 26 1446. Downloaded on 13/11/47 04:29:14 .

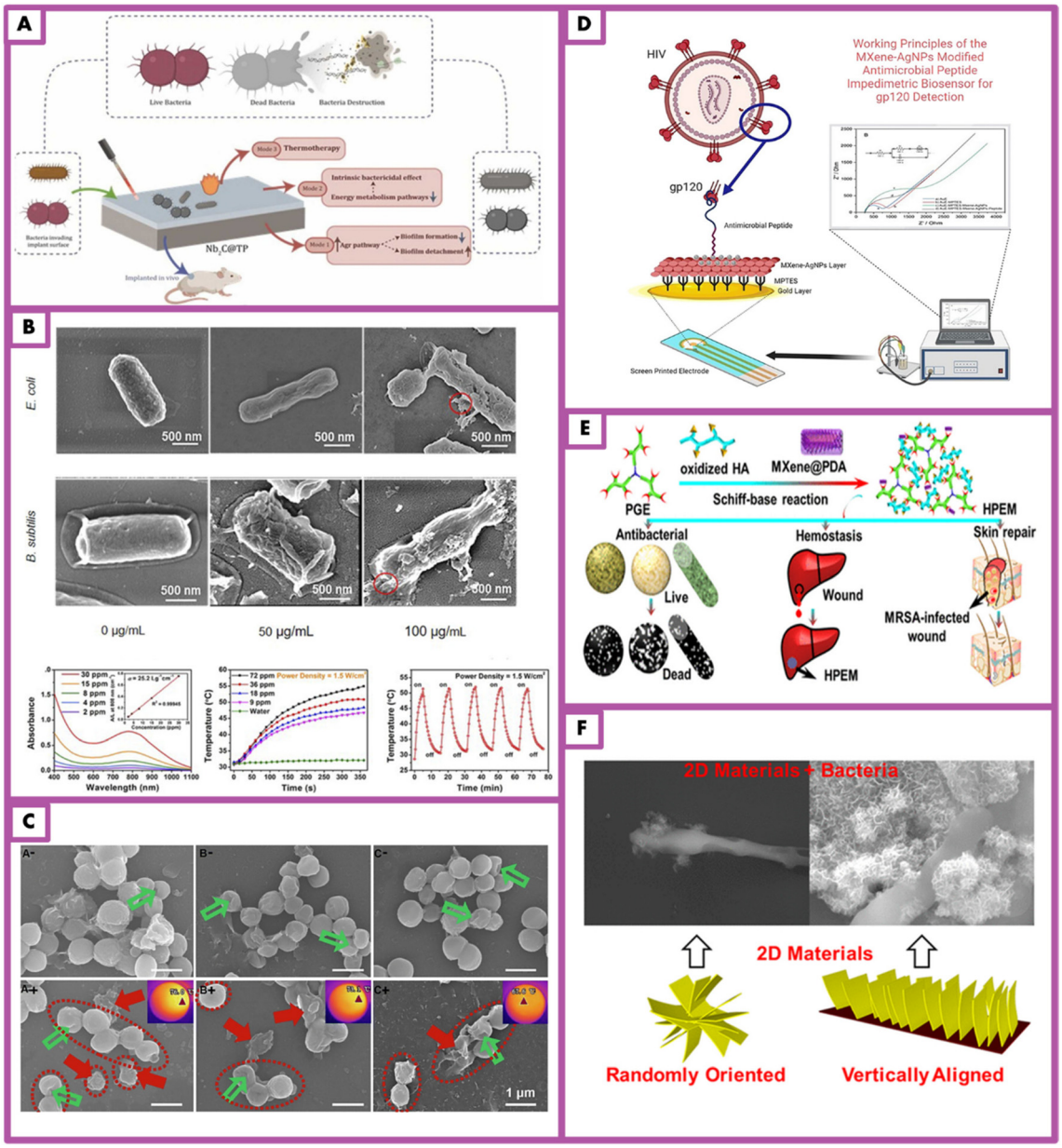


**Fig. 3** (A) Schematic summary, MXenes are shown to exhibit antibacterial, antifungal and antiviral properties, offering potential for infection control, wound healing and advanced medical applications.[123] Copyright 2024. Elsevier. (B) Schematic summary: (a) At concentrations of 50 and 100 μg $mL^{-1}$ MXene, both bacterial types experienced significant cell lysis, as evidenced by noticeable membrane damage and leakage of cytoplasm (indicated by red circles). This illustrates the antibacterial activity of $Ti_3C_2T_x$ MXene.[124] Copyright 2017 Nature (b) MXene composites demonstrated a strong photothermal effect.[125] Copyright 2017 American Chemical Society. (C) Schematic outline: (A–C) Scanning electron microscope (SEM) images of methicillin-resistant *S. aureus* biofilm disrupted by MXenes. Scale bar = 1 μm. Green arrows highlight pits on the cell surface; red arrows point to dead cells showing significant morphological changes; red dotted circles indicate detached *S. aureus* cells or small clusters after biofilm disruption. The symbols "–" and "+" represent conditions without and with NIR exposure, respectively.[111] Copyright 2022 Elsevier. (D) Schematic summary shows an electrochemical biosensor for HIV gp120 detection using MXene, silver nanoparticles and antimicrobial peptides for high sensitivity.[126] Copyright 2024 Elsevier. (E) Schematic summary: MXene is notable for its hydrophilicity, flexibility, and conductivity. It has been shown to be used in a wide range of applications, including environmental, catalysis, biosensors, and drug delivery.[127] Copyright 2023 SPRINGER NATURE. (F) Schematic overview: 2D $MnO_2$ and $MoS_2$ nanomaterials exhibited significant antimicrobial activity by damaging bacterial cell walls, with $MnO_2$ proving to be the most effective.[128] Copyright 2018 American Chemical Society.

mal and photodynamic capabilities, contributing to their dual-action antimicrobial potential. Studies have shown that MXenes, when used in combination with NIR irradiation, can induce significant bacterial damage, including cell death due to the disruption of the bacterial membrane and DNA. The photothermal conversion efficiency of MXene nanosheets has been found to be higher than that of many other nanomaterials, such as gold nanorods, and their stability under

Published on 26 1446. Downloaded on 13/11/47 04:29:14 .

repeated NIR irradiation further underscores their promise as persistent antimicrobial agents. Additionally, the ability of MXenes to generate ROS under light exposure was confirmed through experiments that demonstrated the production of singlet oxygen ($^1O_2$) during NIR irradiation. This ROS generation, coupled with the photothermal effects, results in enhanced antimicrobial efficacy, making MXenes a viable candidate for use in pathogen detection and treatment. The synergistic effects of MXenes in PDT and PTT highlight their potential as effective agents in the battle against drug-resistant bacteria and their possible applications in antimicrobial therapies.[5]

The study conducted by Shamsabadi *et al.*[131] and they investigates the antibacterial properties of $Ti_3C_2T_x$ MXene nanosheets against *Escherichia coli* and *Bacillus subtilis* bacteria. The research demonstrates that the antibacterial activity of the MXene nanosheets is influenced by their size and exposure time. Specifically, smaller nanosheets exhibited higher antibacterial effectiveness against both types of bacteria, with significant cell damage occurring in less than 3 hours. The results indicate that direct physical interactions between the sharp edges of the nanosheets and bacterial cell membranes play a crucial role in antibacterial activity. The study employed fluorescence imaging, flow cytometry, and broth microdilution assays to assess the antibacterial effects, highlighting that the nanosheets cause significant damage to bacterial cells, leading to the release of bacterial DNA and eventual cell dispersion. These findings underscore the potential of MXene-based materials for antibacterial applications in water treatment, medical, and biomedical fields[111] (Fig. 3C).

In a study conducted by Rasool *et al.*[129], the antibacterial properties of $Ti_3C_2T_x$ MXene, MAX phase ($Ti_3AlC_2$), and exfoliated S-$Ti_3C_2T_x$ nanosheets were evaluated against Gram-positive *Bacillus subtilis* and Gram-negative *Escherichia coli* bacteria. The results revealed that S-$Ti_3C_2T_x$ exhibited significantly higher antibacterial activity compared to both F-$Ti_3C_2T_x$ and $Ti_3AlC_2$, emphasizing the important role of MXene thickness in determining antimicrobial effects. Furthermore, the study demonstrated that $Ti_3C_2T_x$ MXenes induced bacterial toxicity by disrupting cell membranes and generating reactive oxygen species (ROS). In another study, $Ti_3C_2T_x$ MXene-based membranes were tested for antibacterial activity against *E. coli* and *B. subtilis*, with fresh membranes showing antibacterial rates of 67% and 73%, respectively, and oxidized membranes achieving more than 99% efficiency. In contrast to these findings, $Ti_2C$ MXenes were found to lack antibacterial activity against *Sarcina*, *S. aureus*, and *Bacillus* sp., with only minimal apoptosis observed. The comparison between the findings of Rasool *et al.*[129] and Jastrzębska *et al.*[132] suggests that the stoichiometry of MXenes plays a pivotal role in determining their antibacterial properties. In a separate investigation, MXene nanosheets with smaller lateral sizes exhibited greater bacterial killing activity, particularly when exposed to bacterial cultures for extended periods. Moreover, the study suggested that the sharp edges of $Ti_3C_2T_x$ MXene nanosheets played a crucial role in bacterial membrane disruption, leading to DNA leakage and eventual cell death. Additionally, Wu *et al.*[136] explored the integration of MXenes with near-infrared light (808 nm), demonstrating its effectiveness against 15 different microbial strains, including antibiotic-resistant strains like MRSA and VRE. This photothermal ablation-based approach was found to be particularly effective in eradicating MRSA biofilms, showcasing the broad potential of MXenes in antimicrobial applications.[136]

A study was conducted to enhance the antibacterial and separation properties of MXene-based 2D membranes for water purification. The research focused on three types of MXene-based composite membranes (GO@MXene, O-g-$C_3N_4$@MXene, and BiOCl@MXene), which were fabricated on polyethersulfone (PES) substrates. The results revealed that the antibacterial activity of these membranes against *Escherichia coli* and *Staphylococcus aureus* was significantly improved, with the BiOCl@MXene composite membrane (M4) showing antibacterial ratios of 50% against *E. coli* and 82.4% against *S. aureus*. Scanning electron microscopy (SEM) analysis demonstrated that the cell density on the modified membranes was notably lower than that on the pure MXene membrane. This study underscores the potential of MXene-based composite membranes for improving antibacterial efficacy in water filtration applications, offering significant advancements in membrane technology by reducing biological fouling.[137]

A study was conducted to develop an antimicrobial peptide-based electrochemical impedance spectroscopy (EIS) biosensor system for the label-free detection of the human immunodeficiency virus (HIV) envelope protein gp120. The biosensor was designed using a gold-coated carbon electrode modified with MXene and silver nanoparticles (AgNPs). Scanning electron microscopy (SEM) confirmed the uniform distribution of MXene and AgNPs on the biosensor surface. The antimicrobial peptide was employed on the electrode surface to reduce the denaturation of the biorecognition receptor, ensuring stable and reliable sensor performance. The biosensor demonstrated a linear detection range of 10–4000 pg $mL^{-1}$ for gp120 with a limit of detection (LOD) of 0.05 pg $mL^{-1}$ and a limit of quantification (LOQ) of 0.14 pg $mL^{-1}$. It exhibited good repeatability when tested with real samples, making it a promising platform for HIV detection in clinical and point-of-care settings[126] (Fig. 3D).

In a study by Chaturvedi *et al.*, a 2D $Ti_3C_2T_x$ MXene-based scaffold (HPEM) was developed to address the challenge of healing MRSA-infected wounds. The multifunctional scaffold exhibited remarkable properties including self-healing behavior, electrical conductivity, tissue adhesion, antibacterial activity (with an antibacterial efficiency of 99.03% against MRSA), and rapid hemostatic capability. The scaffold was fabricated by incorporating poly(glycerol-ethylenimine), $Ti_3C_2T_x$ MXene@polydopamine nanosheets, and oxidized hyaluronic acid. HPEM scaffolds enhanced skin cell proliferation with negligible toxicity and significantly accelerated the healing of MRSA-infected wounds, achieving a 96.31% wound closure rate. The healing process was promoted through anti-inflammatory effects, cell proliferation, angiogenesis, and granula-

 This journal is © The Royal Society of Chemistry 2025

Published on 26 1446. Downloaded on 13/11/47 04:29:14 .

tion tissue formation, further confirming the potential of MXene-based scaffolds for wound healing applications. This study highlights the multifaceted role of MXene-based materials in enhancing the healing of bacterial-infected wounds, particularly MRSA, demonstrating their potential for advanced biomedical applications[127] (Fig. 2E).

A study was conducted to investigate the antibacterial properties of MXene-functionalized graphene (FG) nanocomposites. The nanocomposites, composed of varying ratios of $Ti_3C_2T_x$ and FG (25 : 75%, 50 : 50%, and 75 : 25%), were synthesized and characterized using advanced techniques such as scanning electron microscopy (SEM), energy dispersive X-ray (SEM-EDX), high-resolution transmission electron microscopy (HRTEM), and zeta potential analysis. The cytotoxicity of these nanomaterials was evaluated using immortalized human keratinocytes (HaCaT) cells, and their antibacterial efficacy was tested against both Gram-positive Methicillin-resistant *Staphylococcus aureus* (MRSA) and Gram-negative *Escherichia coli* K1 strains. The results demonstrated potent antibacterial effects against both bacterial strains, while maintaining low cytotoxicity at a concentration of 200 μg $mL^{-1}$, indicating the potential of these materials for biomedical applications.[138]

In a study investigating the antimicrobial properties of 2D nanomaterials, the antimicrobial effects of $MnO_2$ and $MoS_2$ were examined against Gram-positive *Bacillus subtilis* and Gram-negative *Escherichia coli* bacteria. The materials were applied at a concentration of 100 μg $mL^{-1}$ for approximately 3 hours, with vertically aligned and randomly oriented nanomaterials on graphene oxide, reduced graphene oxide, and $Ti_3C_2$ MXene sheets. The bacteria's viability was assessed using flow cytometry and fluorescence imaging, showing that both $MnO_2$ and $MoS_2$ nanosheets exhibited distinct antibacterial activities. In both cases, Gram-positive bacteria experienced greater membrane integrity loss.

Scanning electron microscopy (SEM) revealed that the 2D nanomaterials disrupted bacterial viability by damaging the cell wall and inducing significant morphological changes. The study proposed that the peptidoglycan mesh (PM) in the bacterial wall might be the primary target of the nanomaterials. Among the materials tested, vertically aligned 2D $MnO_2$ nanosheets showed the highest antimicrobial activity, with their edges likely compromising bacterial cell walls upon contact[128] (Fig. 3F).

In a recent study, a wearable, battery-free smart bandage was developed for *in situ* quantitative analysis of bacterial virulence factors to assess wound infections in a timely manner. The bandage enables electrochemical detection of transpeptidase sortase A and pyocyanin, key virulence factors of *S. aureus* and *P. aeruginosa*, which are the most representative bacteria associated with wound infections. The electrode array, fabricated on flexible substrates, was functionalized with $Ti_3C_2T_x$ MXene to enhance the sensitivity of detection. The flexible circuit, enabled with NFC technology, was designed to interface comfortably with the skin, allowing for voltammometric sensing and seamless data transmission to a smartphone for analysis. The study highlights the potential of MXene-based wearable electronics in the point-of-care detection of bacterial virulence factors, positioning MXenes as promising materials in wound infection management. This work further reinforces the growing significance of MXenes in antimicrobial and biosensing applications, particularly for real-time, on-site monitoring of bacterial infections and their virulence, offering a valuable contribution to the field of antimicrobial applications of MXenes.[139]

The study investigates the use of $Ti_3C_2T_x$ MXene nanosheets for photothermal antibacterial therapy, highlighting their potential in treating infectious diseases due to their effective light-conversion capacity and limited bacterial resistance. The research compares the antibacterial efficacy of few-layer (FX) and multi-layer (MX) $Ti_3C_2T_x$ nano-sheets. It was demonstrated that FX exhibited higher cytocompatibility and greater light-to-heat conversion efficiency, while MX showed superior antibacterial activity, particularly against *Staphylococcus aureus* and *Escherichia coli*. In the study, it was shown that at a concentration of 25 μg $mL^{-1}$ of MX, 37% of *E. coli* and 23% of *S. aureus* survived after treatment, while FX had a lesser impact, with 72% of *E. coli* and 46% of *S. aureus* remaining viable. However, at higher concentrations (100 μg $mL^{-1}$), MX exhibited significantly improved bactericidal effects, with only 11% of *E. coli* and 4% of *S. aureus* surviving, while FX had only a mild effect on both species. The near-infrared (NIR)[140] laser treatment further enhanced the antibacterial efficacy of both materials, with 100 μg $mL^{-1}$ of MX combined with 5 minutes of laser treatment at 5.7 W $cm^{-2}$ completely killing both bacterial species. For FX, the treatment with a lower laser intensity (3 W $cm^{-2}$) and the highest concentration of 100 μg $mL^{-1}$ yielded results comparable to MX, with 87% of *E. coli* and 95% of *S. aureus* being killed. This combination of NIR-MXene treatment led to irreversible cell death, which was linked to the loss of cell integrity, as evidenced by DNA release quantification and the observation of bacterial debris.[141]

### 4.2. Antiviral effects of MXenes: interactions with viral structures

The antiviral properties of MXenes offer significant potential for their biomedical applications. MXenes, particularly those with hydrophilic characteristics, possess negative surface functional groups that allow them to interact with viral particles. This interaction effectively traps the viruses and either inactivates or kills them by binding to the spike proteins on the virus surface. The adsorption between the MXene surface and the amino acids in the peplomers leads to the retention of the virus, followed by its inactivation. A study by Unal *et al.*[142] investigated the antiviral efficacy of $Ti_3C_2T_x$ MXene against various SARS-CoV-2 clades (including GR, GH, and S) using Vero E6 cell cultures infected with the virus. The results showed a significant reduction in viral copy numbers by 99% for the GR clade, even at a high dilution (1 : 3125). In contrast, other clades showed no significant reduction. The antiviral effectiveness was linked to the specific viral genotype and mutations, underlining the importance of considering these factors when evaluating the efficacy of nanomaterials. The

Published on 26 1446. Downloaded on 13/11/47 04:29:14 .

study also highlighted that $Ti_3C_2T_x$ MXene exhibited minimal cytotoxicity while significantly improving the viability of infected cells. Further comparison of $Ti_3C_2T_x$, $Ta_4C_3T_x$, $Mo_2Ti_2C_3T_x$, and $Nb_4C_3T_x$ MXenes revealed that $Ti_3C_2T_x$ was the most potent antiviral material, achieving a 99% reduction in viral copy numbers at a concentration as low as 0.32 μg $ml^{-1}$. On the other hand, $Mo2Ti_2C_3T_x$ and other MXenes demonstrated lower antiviral activities. This finding was supported by additional experiments with $TiO_2$ nanoparticles, which confirmed that the antiviral activity was attributed to the $Ti_3C_2T_x$ MXene and not the titanium particles. Another study by Ghasemy *et al.*[143] explored the interactions between $Mo_2C$, $Ti_2C$, and $Mn_2C$ MXene nanosheets and the spike proteins of the SARS-CoV-2 virus. The results indicated that MXenes could not only adsorb the spike proteins but also modify their secondary structure, preventing the virus from binding to the $ACE_2$ receptors on human cells, which are responsible for viral entry. Among the MXenes tested, $Mn_2C$ MXene exhibited the highest potential for inhibiting viral infection.[24]

The challenges posed by sudden viral outbreaks, such as COVID-19, H1N1 flu, and H5N1 flu, have emphasized the critical need for rapid and cost-effective diagnostic solutions. According to a recent study, the use of MXenes as sensing materials for developing virus-detecting biosensors has shown significant potential in addressing these challenges. MXenes offer distinct advantages, including high conductivity, tunable electrical and optical properties, abundant functional groups, and a large specific surface area, making them ideal candidates for biosensor development. This research highlights the application of MXene-based biosensors for detecting biomolecules such as viruses, enzymes, antibodies, proteins, and nucleic acids. Despite their advantages, certain limitations, including extended detection times and high costs associated with current biosensing technologies, remain. To overcome these, the study discusses advanced strategies integrating MXene-based biosensors with technologies such as artificial intelligence, the Internet of Things, 5G communication, and cloud computing. These advancements are expected to contribute to the development of intelligent, point-of-care diagnostic tools for viral infections.[26]

By Khatami *et al.*[144] the antimicrobial and environmental remediation potential of MXene materials was explored through the development of a biocatalytic system for degrading recalcitrant pollutants, specifically antiretroviral drugs (ARVs) in wastewater. The research targeted efavirenz, a model ARV, as a persistent pollutant commonly introduced into aquatic systems through inefficient pharmaceutical waste management. The study utilized $Ti_2N$ MXene, synthesized through selective etching of the $Ti_2A_lN$ MAX phase, as a support material for the covalent immobilization of laccase enzymes derived from Rhus vernificera and Trametes versicolor. The structural and chemical properties of the synthesized MXene were characterized using techniques such as Raman spectroscopy, XRD, FTIR, EDS, and XPS, which confirmed the successful formation of $Ti_2NT_x$ MXene with surface terminations including O, F, and OH groups. The immobilization of laccase on MXene surfaces was optimized using glutaraldehyde and hexamethylene diamine (HMDA) as linkers, with HMDA demonstrating minimal impact on enzyme immobilization but enhancing enzyme activity. Among the two laccase isoenzymes studied, Trametes versicolor laccase showed superior enzyme activity and loading efficiency, making it suitable for application studies. The enzymatic degradation of efavirenz was evaluated under optimal conditions, revealing that the immobilized laccase achieved up to 63% degradation in the presence of a mediator (ABTS), compared to less than 30% without assistance. Additionally, the immobilization process improved the pH tolerance of the enzyme, enabling its functionality in neutral wastewater conditions (pH 7). The study further integrated the immobilized laccase into a 3L bioreactor operated at pH 7, achieving significant degradation efficiencies (~73% at 25 ppm efavirenz concentration) in simulated wastewater treatment conditions. These results demonstrated the potential of MXene-supported biocatalysts as an environmentally friendly and efficient solution for the removal of persistent organic pollutants from wastewater, highlighting their broader applicability in antimicrobial and environmental remediation systems.[144]

The antiviral properties of MXene-based nanocomposites have been highlighted in a study conducted by other researchers. In their work, two-dimensional (2D) MXene nanocomposites modified with a heparan sulfate analogue (sodium 3-mercapto-1-propanesulfonate, MPS), referred to as $Ti_3C_2$-Au-MPS, were synthesized and investigated for their potential to prevent viral infections. The study evaluated the effects of these nanocomposites using severe acute respiratory syndrome coronavirus 2 (SARS-CoV-2) pseudovirus and porcine reproductive and respiratory syndrome virus (PRRSV) as model systems. The $Ti_3C_2$-Au-MPS nanocomposites were reported to interfere with multiple stages of viral proliferation, including direct interaction with virions and inhibition of their adsorption and penetration into host cells. Furthermore, their effectiveness against SARS-CoV-2 pseudovirus was demonstrated through a significant reduction in reporter gene expression levels, such as GFP and luciferase. These findings underscore the broad-spectrum antiviral potential of MXene-based nanocomposites, particularly against viruses reliant on heparan sulfate receptors. This study contributes to the understanding of MXenes' antiviral mechanisms and their potential applications in virology.[145]

In previous research, the synthesis of low-density, porous, and lightweight MXene foams with advanced properties for biomedical applications was reported. These MXene foams demonstrated particulate filtration capabilities, which align with the requirements for ensuring pure air. Such properties were noted as particularly beneficial during the COVID-19 pandemic due to the widespread use of face masks as a preventive measure against viral contamination. However, it was highlighted that once viruses adhere to the outer layers of face masks, they can remain active for extended periods, posing risks related to handling and disposal. To address this,

 This journal is © The Royal Society of Chemistry 2025

Published on 26 1446. Downloaded on 13/11/47 04:29:14 .

MXene-based face masks were developed, which not only capture viruses but also inactivate them due to the intrinsic antiviral properties of MXenes. Furthermore, it was suggested that similar virus-inactivation strategies could be employed by coating MXenes on personal protective equipment (PPE) and other medical devices. Applications such as MXene-coated PPE kits, face shields, and transparent medical spectacles with antiviral properties were proposed as methods to reduce infection rates, particularly among asymptomatic individuals infected with COVID-19.[24]

# 5. MXene-based therapeutic platforms in microbiology and virology

## 5.1. Drug delivery systems using MXenes for targeted therapy

MXene is a highly adaptable material with unique features, including excellent electrical conductivity, mechanical strength, magnetic properties, and outstanding optical characteristics. Composed of surface-modified carbides, MXenes are two-dimensional compounds known for their large surface area and hydrophilic nature, making them ideal candidates for drug delivery systems that require high drug loading capacities. Incorporating MXenes into hydrogel matrices has been shown to improve drug loading, provide controlled release profiles, and enhance stability. This integration enables the regulated release of MXene nanoparticles, promoting prolonged antibacterial and antiviral effects. As a result, it prevents bacterial colonization, biofilm formation, and the entry of viruses into host cells. The distinctive properties and customizable surface chemistry of MXene-based hydrogels [146] position them as a promising platform for both drug delivery and antimicrobial applications. These hydrogels support efficient drug loading, controlled release, and targeted therapeutic interventions, while their natural antimicrobial and antiviral properties present opportunities for the development of effective treatments. For example, in this study, have developed an innovative nanocarrier for drug delivery using a new MXene material. The MXene nanosheets were functionalized with 3,3′-diselanediildipropionic acid and subsequently conjugated with doxorubicin, a model chemotherapy drug. The nanosheets were thoroughly characterized through several methods, including microscopy, spectroscopy, and X-ray diffraction analysis. The drug loading capacity and encapsulation efficiency were assessed, and the dimensions of the nanosheets were also measured. The drug release profile demonstrated responsiveness to both reactive oxygen species and pH changes. Furthermore, these nanosheets showed significant antibacterial activity against both Gram-negative and Gram-positive bacteria. These results highlight the potential of MXene-based nanocarriers for targeted drug delivery and antimicrobial applications[147] (Fig. 4A).

Koohkhezri *et al.*[153] introduces a method for creating fibrous scaffolds capable of delivering natural drugs and herbal compounds, aimed at advancing tissue regeneration and wound healing in personalized medicine. The scaffolds were fabricated using coaxial electrospinning, with polycaprolactone (PCL) and pectin nanofibers forming the core–shell structure. Berberine chloride, a plant-derived compound with various therapeutic properties, served as a model drug. To improve the mechanical strength of the core fibers, poly(vinyl alcohol) (PVA) was combined with pectin. The shell was modified with two-dimensional $Ti_3C_2T_x$ (MXene) nanosheets and crosslinked *via* both covalent and ionic methods. Structural analysis confirmed the successful production of bead-free fibers, with diameters ranging from 160 to 350 nm depending on the composition. The addition of berberine and MXene to the fibers resulted in an increase in fiber diameter. Drug release from the fibers followed a two-phase mechanism, beginning with a burst release in the first 24 hours, followed by sustained release over a two-week period. The release mechanisms were identified as case-II relaxation in the first phase and quasi-Fickian diffusion in the second phase. Incorporating MXene into the shell of the fibers further extended the release time. The mechanical strength of the scaffolds was significantly improved, with increases of 7 times in wet conditions and 4 times in dry conditions. Biocompatibility assessments using $L_{929}$ cells demonstrated excellent cell adhesion and compatibility. Antibacterial testing against *Escherichia coli* revealed that the inclusion of MXene enhanced antibacterial activity by 30%. These results suggest that the developed biocomposite scaffolds have promising potential for use in the creation of advanced drug-releasing wound dressings.[154] In conclusion, MXene-based therapeutic platforms hold significant promise for antibacterial and antiviral treatments, enabling targeted and controlled drug delivery. The adaptable surface characteristics and inherent antimicrobial properties of MXene pave the way for the creation of effective treatment approaches in both virology and microbiology.[153]

## 5.2. MXene-based photothermal and photodynamic therapies

MXenes and their associated nanocomposites have attracted considerable attention due to their unique physicochemical properties, including high surface area, ease of synthesis and functionalisation, and significant drug loading capacity. These properties make them ideal candidates for various photomedical applications. MXenes have shown promise in a wide range of therapeutic approaches including imaging, photothermal cancer therapy and tumour ablation. Non-invasive theranostic strategies integrating photothermal, photodynamic and magnetic therapies, as well as remote drug and gene delivery, have been developed for the effective diagnosis and treatment of cancer. MXene-based materials have significant potential for photothermal and photodynamic therapies and photoacoustic imaging in cancer treatment. However, further research is needed to explore hybridization and surface modification of MXenes to improve their biocompatibility, functionality and stability. It is especially important to prioritize toxicological evaluations, long-term biosafety studies and clinical translation. Today, a lot of work has been done to improve this. For

Published on 26 1446. Downloaded on 13/11/47 04:29:14 .

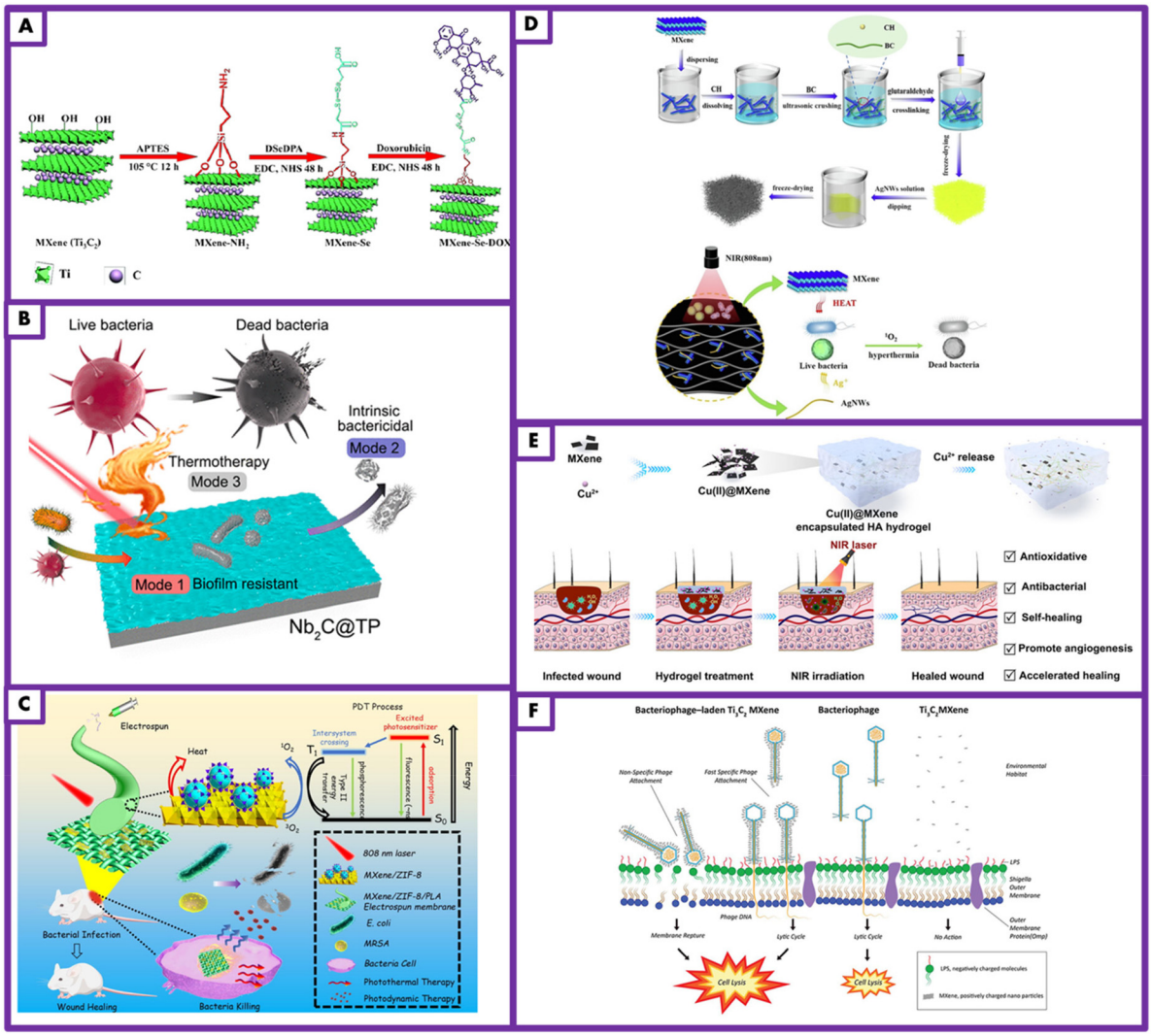


**Fig. 4** (A) Schematic summary illustrates the synthesis process of MXene-Se-DOX nanosheets.[147] Copyright 2022 MDPI. (B) Schematic summary, the $Nb_2C$@TP MXene implant highlights its ability to inhibit biofilm formation, eliminate bacteria and enhance tissue regeneration.[148] Copyright 2020 American Chemical Society. (C) Schematic overview of the MZ-8/PLA composite illustrates its ability to combat resistant bacterial infections and promote wound healing. This is accomplished through its antibacterial properties, which are activated by photothermal and photodynamic therapies.[149] Copyright 2021 Elsevier. (D) Schematic summary demonstrates the creation of a multifunctional biomass composite aerogel by co-modifying MXene and Ag nanowires (AgNWs) onto a bacterial cellulose/chitosan (BC/CH) composite aerogel. This simple and effective approach is ideal for health monitoring and photo-thermal antibacterial uses.[150] Copyright 2022 Elsevier. (E) Schematic summary outlines the preparation and use of Cu (II)@MXene photothermal hydrogels. (a) The Cu(II)@MXene complex was formed through electrostatic aggregation, and the hydrogels were created by combining Cu(II)@MXene suspension with OHA and HA-ADH solutions. (b) These hydrogels can be injected onto infected wounds, forming a protective layer that supports the healing process.[151] Copyright 2023 Frontiers. (F) Schematic summary shows that bacteriophages loaded with $Ti_3C_2$ MXene effectively target bacteria, reducing contamination and preventing bacterial regrowth.[152] Copyright 2022 Elsevier.

example, Yu *et al.*[155] the potential of combining PTT and PDT was explored by incorporating indocyanine green (ICG) onto $Ti_3C_2T_x$ MXene nanosheets, which serve as both photothermal agents and carriers. In the absence of near-infrared (NIR) irradiation, neither MXene, ICG, nor ICG-loaded MXene (ICG-MXene) exhibited notable antibacterial effects against methicillin-resistant *Staphylococcus aureus* (MRSA). However, under NIR exposure, the viability of MRSA significantly decreased, with MXene causing a 45% reduction, ICG reducing viability by 66%, and ICG-MXene achieving complete bacterial eradication. The enhanced antibacterial effect observed with ICG-MXene was attributed to the combined action of MXene's photothermal effect (elevating temperature) and ICG's photodynamic activity (generating reactive oxygen species). These results suggest that MXene could be effectively utilized as a carrier for photosensitizers, enabling a synergistic PTT/PDT treatment approach for bacterial infections.[155]

Wu *et al.*[156] a new 0D/2D Schottky heterojunction has been created as an environmentally friendly and antibiotic-free approach for treating bacterial infections. This hybrid

 This journal is © The Royal Society of Chemistry 2025

Published on 26 1446. Downloaded on 13/11/47 04:29:14 .

material, consisting of $Ag_2S$ and $Ti_3C_2$, demonstrated impressive antibacterial activity, achieving a 99.99% reduction in bacteria within 20 minutes under 808 nm near-infrared (NIR) light exposure. The enhanced antibacterial effects of this material are attributed to the synergy between its photocatalytic and photothermal properties. The researchers used density functional theory (DFT) calculations to explain the underlying mechanism, revealing that charge redistribution at the $Ag_2S/Ti_3C_2$ interface led to an upward shift in the $Ag_2S$ energy band. Additionally, the material's antibacterial effectiveness was largely due to the rapid transfer of photoexcited electrons from $Ag_2S$ to $Ti_3C_2$, facilitated by the higher conduction band energy of $Ag_2S$ compared to the Fermi level of $Ti_3C_2$, along with the excellent electrical conductivity of $Ag_2S$. *In vitro* and *in vivo* experiments confirmed the hybrid's strong antibacterial activity against *Staphylococcus aureus* and its excellent biocompatibility. This hybrid is proposed as a promising platform for rapid, environmentally friendly treatment of bacterial infections using NIR light.[156]

Liu *et al.*[157] have developed fibrous photothermal membranes coated with MXene, designed to efficiently generate water vapor for water treatment through solar-powered evaporation. These membranes exhibit high light absorption efficiency across a wide range of solar spectra, achieving a water evaporation rate of 1.44 kg $m^{-2}$ $h^{-1}$ under sunlight. In addition, the membranes show strong antibacterial activity, reducing bacterial growth by 99.9%, and remain stable even under ultrasonication and mechanical agitation. A combination of MXenes and cobalt nanowires was utilized to fight pathogenic bacteria through a synergistic approach, leveraging near-infrared-induced reactive oxygen species (ROS) and hyperthermia. The integration of plasmonic cobalt nanowires significantly enhanced the antibacterial performance of the MXene-based photothermal membranes, resulting in a greater than 90% reduction in bacterial growth within 20 minutes. Mechanistic studies revealed that upon NIR laser illumination, electron excitation occurs, leading to reactions with oxygen that generate ROS. These results highlight the promising potential of MXene-based membranes and nanowires as effective solutions for addressing antibiotic resistance.[157]

Yang *et al.*[148] developed a clinical implant made of two-dimensional niobium carbide ($Nb_2C$) MXene titanium plates ($Nb_2C$@TP) that exhibits a broad spectrum of antimicrobial properties. This advanced implant can effectively disrupt biofilms, prevent biofilm formation, and promote biofilm detachment, leading to bacterial eradication. These effects are achieved by down-regulating bacterial energy metabolism pathways and activating accessory gene regulators. Additionally, the implant enhances the susceptibility of bacteria to elimination *via* photothermal transduction, which lowers the required temperature and minimizes potential tissue damage. The $Nb_2C$@TP implant also shows promise in reducing pro-inflammatory responses by scavenging excess reactive oxygen species in infectious environments. This process not only reduces unwanted inflammation but also aids in angiogenesis and tissue remodeling. Given the limitations of current antimicrobial and anti-biofilm treatments, the development of nanomedicine-based approaches like the $Nb_2C$@TP implant provides a promising and effective solution to the challenges posed by difficult-to-treat bacterial infections, biofilms resistant to penetration, and antibiotic resistance (Fig. 4B).[148]

Zheng *et al.*[158] have explored the potential of MXenes, particularly $Ti_2C_2$, as nanomedicines with antimicrobial properties. However, the antibacterial effectiveness of $Ti_3C_2$ MXene is limited by its weak interaction with bacteria and suboptimal performance in photothermal therapy. To overcome these challenges, a hybrid hydrogel combining the cationic antibiotic ciprofloxacin with $Ti_3C_2$ MXene has been developed. This hybrid hydrogel demonstrated the ability to effectively capture and eliminate bacteria through the combined action of chemotherapy and photothermal therapy. *In vitro* results showed that the hybrid hydrogel achieved over 99.99999% bactericidal efficacy against methicillin-resistant *Staphylococcus aureus* (MRSA). Additionally, in an MRSA-induced mouse abscess model, the hydrogel provided potent sterilization and long-lasting bacterial inhibition, preventing bacterial regrowth after photothermal treatment. These findings highlight the potential of MXene-based hybrid hydrogels to improve the therapeutic outcomes of antimicrobial therapies.[158]

Zhang *et al.*[149] a composite membrane, named MZ-8/PLA, has been developed to address bacterial wound infections. The membrane is composed of titanium carbide, zeolite imidazole framework-8 (ZIF-8), and polylactic acid (PLA). MZ-8/PLA demonstrated impressive bactericidal properties, with a photothermal conversion efficiency of 80.5%. In addition to its antibacterial activity, the membrane showed promising antitumor effects when combined with photodynamic and photothermal therapies. It enhanced laser activation by facilitating intermolecular charge transfer, stabilizing excited states, and improving antibacterial efficacy. When integrated into electrospun scaffolds, the MZ-8/PLA membrane exhibited strong photothermal and photodynamic therapeutic properties upon laser irradiation. It achieved significant antibacterial effects, with a 99.9% reduction in *Escherichia coli* and 99.8% reduction in methicillin-resistant *Staphylococcus aureus* (MRSA). *In vivo* studies further confirmed that MZ-8/PLA could accelerate wound healing in bacterial-infected areas without resistance. This study highlights the potential of MZ-8/PLA as a multifunctional therapeutic platform for combating drug-resistant bacteria and enhancing the treatment of bacterial infections in wounds[149] (Fig. 4C).

Fu *et al.*[150] investigated the creation of a multifunctional biomass composite aerogel obtained by co-modifying MXene and silver nanowires (AgNWs) on a bacterial cellulose/chitosan (BC/CH) aerogel through a combination of physical mixing, lyophilisation and electrostatic adsorption. The resulting BC/CH/MXene/AgNWs composite aerogel shows promise for use both as a health monitoring sensor and as a photo-thermal antibacterial material. As a health sensor, it showed high sensitivity, fast response time and excellent cyclic stability. It has been successfully applied to monitor various human body

Published on 26 1446. Downloaded on 13/11/47 04:29:14 .

movements, including foot, elbow and wrist movements, breathing and throat vibration associated with pronunciation. Furthermore, the composite aerogel exhibited outstanding photothermal conversion, rapidly reaching temperatures above 60 °C within 60 s under near-infrared (NIR) laser irradiation (808 nm, 0.6 W $cm^{-2}$). The BC/CH/MXene/AgNW aerogel achieved near 100% sterilisation as a result of the synergistic antibacterial effect resulting from the combined effects of CH/AgNWs and the photothermal antibacterial properties of MXene. This new aerogel shows improved sensitisation and superior antibacterial performance compared to conventional biomass aerogels. Its multifunctionality positions it as a promising candidate for integration into wearable and implantable health monitoring devices (Fig. 4D).[150]

Liu *et al.*[151] developed a Cu(II)@MXene photothermal complex *via* electrostatic self-assembly between $Cu^{2+}$ ions and MXene. This complex was incorporated into a hyaluronic acid (HA) hydrogel to create an antibacterial dressing. The dressing demonstrates rapid adhesion, self-healing properties, and injectability, making it versatile for various wound shapes and providing long-lasting protection. Moreover, the Cu(II)@MXene complex, which is easily synthesized, functions as a photothermal antibacterial barrier, ROS scavenger, and angiogenesis promoter, thus promoting faster wound healing. *In vivo* testing confirmed that the Cu(II)@MXene photothermal hydrogel dressing significantly improved inflammatory responses, collagen accumulation, blood vessel formation, and wound closure (Fig. 4E).[151]

Ding *et al.*[159] a near-infrared (NIR)-activated multifunctional antimicrobial nanospray (MXene/ZIF-90@ICG) was developed by integrating ZIF-90@ICG nanoparticles onto MXene-$NH_2$ nanosheets. This MXene/ZIF-90@ICG composite allows for the controlled release of antimicrobial agents, including MXenes, indocyanine green (ICG), and $Zn^{2+}$, in response to changes in pH and ATP levels in the bacterial infection microenvironment. When exposed to NIR radiation, the combination of MXenes, $Zn^{2+}$, and ICG generated a significant amount of reactive oxygen species (ROS) and produced heat, thereby enhancing the antimicrobial activity of both photodynamic therapy (PDT) and photothermal therapy (PTT). Additionally, NIR exposure facilitated the further release of ICG and $Zn^{2+}$, thereby achieving a multimodal synergistic antibacterial effect involving PDT, PTT, and $Zn^{2+}$. The incorporation of MXenes also improved the dispersion of the antimicrobial nanoparticles in aqueous solutions, making MXene/ZIF-90@ICG a promising candidate for use as a nanospray. Notably, *in vivo* studies using a subcutaneous *Staphylococcus aureus* infection model demonstrated the antimicrobial efficacy of MXene/ZIF-90@ICG under NIR activation, which also promoted wound healing while maintaining favorable biosafety. Consequently, MXene/ZIF-90@ICG shows significant potential as an innovative nanospray for adaptive, multimodal antibacterial applications activated by NIR.[159]

Zhao *et al.*[160] reports the successful synthesis of vanadium carbide-based ($V_2CT_x$-Au) nanostructures through electrostatic self-assembly, designed for the direct detection and eradication of bacteria. These nanostructures can be used directly for label-free bacterial detection *via* surface-enhanced Raman spectroscopy, eliminating the need for complex processing steps. Photothermal experiments showed that the $V_2CT_x$-Au nanostructures could heat up to over 50 °C in just 200 seconds, with a photothermal conversion efficiency of 37.82%. Additionally, experiments confirmed that the nanostructures generate reactive oxygen species (ROS), including $O_2^{\bullet-}$ and $1O_2$. When combined with scanning electron microscopy (SEM) images of bacteria, the results indicated that $V_2CT_x$-Au nanostructures effectively produced antibacterial effects through photothermal therapy under 808 nm laser irradiation and exhibited synergistic antibacterial properties *via* photodynamic therapy. The survival rates of *Escherichia coli (E. coli)* and extended-spectrum β-lactamase *Escherichia coli (ESBL-E. coli)* were reduced to 6.88% and 1.58%, respectively. Moreover, cytotoxicity and hemolytic assays confirmed that the $V_2CT_x$-Au nanostructures demonstrated excellent biocompatibility. This study presents a promising method for rapid, label-free bacterial detection and antibiotic-free sterilization, which could help address the growing issue of bacterial infections, especially those caused by drug-resistant strains.[160]

In conclusion, MXene-based photothermal and photodynamic therapies offer an effective and innovative approach to the treatment of cancer and other infectious diseases. However, further research into the biocompatibility, safety and clinical efficacy of these treatment modalities is essential to ensure the widespread application of these technologies in the future.

### 5.3. Potential of MXenes in antimicrobial and antiviral coatings

In the development of antimicrobial and antiviral treatment strategies, MXenes, a class of two-dimensional materials, have the potential to play an important role due to their unique properties. Recent studies have revealed significant findings indicating how the advantages of MXenes, including high colloidal stability, photocatalytic activity, excellent electrical conductivity, and surface modification capabilities, can be leveraged in the development of antimicrobial and antiviral coatings. These properties render MXenes an even more crucial component in the development of next-generation coating materials, particularly in the context of combating infections. A plethora of applications have already been documented, including:

Tong *et al.*[145] explored the antiviral properties of MXene nanocomposites modified with a heparan sulfate analogue (MPS), specifically the $Ti_3C_2$-Au-MPS nanocomposites, against two model viruses: the SARS-CoV-2 pseudovirus and PRRSV. The study revealed that these nanocomposites exhibit significant antiviral activity against both viruses. For PRRSV, the $Ti_3C_2$-Au-MPS nanocomposites were shown to directly interact with the viral particles, effectively preventing their adsorption and entry into host cells. In the case of the SARS-CoV-2 pseudovirus, the nanocomposites demonstrated a strong inhibitory effect on viral infection, as evidenced by a

 This journal is © The Royal Society of Chemistry 2025

Published on 26 1446. Downloaded on 13/11/47 04:29:14 .

considerable reduction in the levels of GFP and luciferase reporter genes. These results suggest that $Ti_3C_2$-Au-MPS nanocomposites could offer a broad-spectrum antiviral effect, particularly against viruses that utilize heparan sulfate receptors. The study highlights the promising potential of MXene-based nanocomposites for antiviral applications and calls for further investigation in this area.[145]

Mansoorianfar *et al.*[152] $Ti_3C_2$ MXene nanofragments, approximately 20 nm in size, were electrostatically bound to well-characterized bacteriophages, creating a novel antibacterial agent in the form of a modified viral vector designed for use in high-risk bacterial environments. When the MXene concentration exceeds the minimum inhibitory concentration (MIC), the MXene-functionalized bacteriophage demonstrates significantly increased antibacterial activity. This enhanced activity results from the high specificity of the bacteriophage for host receptors and the ability to target bacterial surfaces with negative charges, compared to the bacteriophage alone. Additionally, the positive charges introduced on the MXene surface guide the nanofragments towards the negative charge of bacterial surfaces. The primary mechanisms involve the bacteriophage's ability to specifically target bacteria, often leading to host lysis, along with the physical interaction of MXene nanofragments with bacterial cell membranes, which helps disrupt the bacterial cell wall. The findings show that $Ti_3C_2$ MXene substantially improves bacteriophage adsorption and stability during long-term cultivation in aquatic environments, providing enhanced antibacterial activity against targeted bacterial cells. The MXene-loaded bacteriophage rapidly and efficiently binds to bacterial host cells, demonstrating a high antibacterial potential and reducing contamination by 99.99% in water samples. Notably, no regrowth of target bacteria was observed during the experimental period, with bacterial counts remaining consistently below detectable levels. This study highlights a novel approach to creating an antibacterial agent using a straightforward, one-step technique, avoiding the limitations commonly associated with conventional post-treatment methods (Fig. 4F).[152]

Naser *et al.*[161] investigated the potential of MXene-based nanostructures in addressing microbial threats, highlighting their various antimicrobial mechanisms. MXenes exhibit unique properties that make them highly suitable for therapeutic applications, alongside scalable production and various synthesis techniques. Key characterization methods such as X-ray diffraction (XRD), Raman spectroscopy, scanning electron microscopy (SEM), transmission electron microscopy (TEM), Fourier transform infrared spectroscopy (FTIR), X-ray photoelectron spectroscopy (XPS), and Brunauer–Emmett–Teller (BET) analysis are utilized to detail their structural and functional attributes. These materials have shown effectiveness against bacterial, viral, and fungal infections by mechanisms including membrane disruption and the induction of oxidative stress. Although there are challenges in translating this technology into practical applications, MXene-based nanostructures present a viable option as broad-spectrum antimicrobial agents, with potential uses in drug delivery systems and diagnostic tools. This positions MXenes as a promising approach to enhancing infection control in global healthcare settings.[161]

Salmi *et al.*[138] synthesized graphene nanocomposites by varying the proportions of MXene-functionalized graphene (FG) and $Ti_3C_2T_x$. The nanocomposites were thoroughly characterized using various microscopy techniques, including scanning electron microscopy (SEM), energy-dispersive X-ray spectroscopy (EDX), and high-resolution transmission electron microscopy (HRTEM), along with zeta potential analysis. The cytotoxicity of the composites was assessed on immortalized human keratinocyte (HaCaT) cells at different time intervals. The antibacterial properties were tested against methicillin-resistant *Staphylococcus aureus* (MRSA) and neuropathogenic *Escherichia coli* $K_1$. The results showed that the nanocomposites displayed strong antibacterial activity against both MRSA and *E. coli* $K_1$, while maintaining low cytotoxicity towards HaCaT cells at a concentration of 200 μg $mL^{-1}$. These findings suggest that the nanocomposites possess promising antimicrobial properties and biocompatibility, making them suitable candidates for biomedical applications.[138]

Liu *et al.*[162] conducted to evaluate the performance of an electromagnetically enhanced air filtration system in deactivating a model viral species ($MS_2$) in a simulated bioaerosol setting. The system utilized a nonwoven fabric filter coated with MXene ($Ti_3C_2T_x$), a two-dimensional material that functions as a catalyst to absorb electromagnetic radiation, generate localized heating, and produce an electromagnetic field for microbial inactivation. The results showed that the MXene-coated filter significantly improved viral removal efficiency, achieving a log removal value of 3.4 under an electromagnetic power density of 3.4 W $cm^{-2}$. In contrast, the uncoated filter only reached a log removal of 0.3. The primary mechanism for viral deactivation was local heating, with the filter surface temperature reaching 72.2 °C under the electromagnetic field. The study also investigated the non-thermal effects contributing to enhanced viral capture, using COMSOL simulation to explore potential pathogen transmission pathways. These findings provide valuable insights into airborne pathogen control and offer a better understanding of their transmission, with potential implications for public health and the development of advanced air filtration systems, particularly in light of the ongoing pandemic.[162]

In conclusion, MXenes, with their superior properties and high efficiency for antimicrobial and antiviral coatings, will occupy an important place in the healthcare field in the future, providing an effective strategy for the control of infections (Table 3).

## 6. Current challenges in MXene applications for microbial and viral targets

Despite the evident potential of MXenes and MXene-based materials in combating microbes and viruses, their clinical

Published on 26 1446. Downloaded on 13/11/47 04:29:14 .

Table 3 Summarises the advantages, disadvantages, applications, research status and potential future applications of MXene based therapeutic platforms in microbiology and virology

| | Description | Applications | Advantages | Disadvantages | Research status | Potential future applications | Ref. |
|---|---|---|---|---|---|---|---|
| Drug delivery systems using MXenes for targeted therapy | MXene-based drug delivery systems enhance therapeutic effects by directly targeting therapeutic agents to infected regions. This is particularly important for antibiotic-resistant bacteria and non-responsive viruses | MXene-based drug delivery can be used for targeted transport of antibiotics and antivirals, especially for bacterial infections (MRSA, *E. coli*) and viral diseases (HIV, influenza) | Targeted therapy increases treatment efficacy, reduces side effects, allows for controlled drug release, and improves overall treatment outcomes | Limited clinical trials, potential incompatibility with some drugs, and degradation issues remain concerns | Demonstrated success in preclinical studies, though clinical testing is still in progress | MXene-based systems could offer effective treatments for antibiotic-resistant microorganisms, and targeted therapy for viral diseases like HIV and influenza in the future | 163 |
| MXene-based photothermal and photodynamic therapies | MXenes can convert light energy into heat for photothermal therapy and generate free radicals for photodynamic therapy, leading to the elimination of microorganisms and viruses | Photothermal therapy is effective against antibiotic-resistant bacteria (MRSA), and photodynamic therapy can be used for viruses like HIV and influenza | Non-invasive, minimizes side effects, environmentally friendly, and sustainable treatment method | Limited tissue penetration of light energy, potential damage to non-target cells, and restricted effect area | High efficacy demonstrated in preclinical tests, but clinical trials are still limited | In the future, photothermal therapy could play a crucial role in treating antibiotic-resistant infections, and photodynamic therapy could be a breakthrough in viral disease treatments | 164 |
| Potential of MXenes in antimicrobial and antiviral coatings | MXene-based coatings prevent the proliferation of microorganisms (bacteria, fungi) and viruses (HIV, influenza) on surfaces, offering significant protection in medical environments and equipment | Antimicrobial and antiviral coatings on medical devices, personal protective equipment (masks, gloves), and hospital surfaces to prevent pathogen spread | Long-lasting effectiveness, broad-spectrum microorganism and virus elimination capabilities, and environmentally safe | Challenges in maintaining long-term stability of coatings and potential toxicity of some MXene components | Effectiveness proven in clinical tests, and research for commercial products is ongoing | Antimicrobial/antiviral coatings could become widespread in medical devices, personal protective equipment, and food safety applications | 165 |

application is impeded by challenges pertaining to biocompatibility, toxicity, surface modification, and production methodologies. The biological effectiveness of these materials is influenced by factors such as size, shape, and surface characteristics, underscoring the need for further research to substantiate their safety and feasibility for manufacturing.

MXenes and MXene-based materials have attracted significant interest due to their potential as versatile agents in the treatment of microbial and viral infections. However, several challenges must be addressed before these materials can be fully utilized in biomedical and clinical settings. One of the primary concerns is determining the biocompatibility and toxicological effects of MXenes. Research has shown that certain MXene derivatives may cause cellular damage and exhibit toxic effects. For example, MXene nanosheets have been found to negatively impact embryonic development and angiogenesis, with these effects being concentration dependent. Consequently, it is crucial to better understand the safety and toxicity mechanisms associated with MXenes.[166]

Moreover, the performance of MXenes in biological systems is influenced by various factors, including their size, shape, surface charge, and the modifications applied to their surface. These properties can significantly affect the materials' antimicrobial and antiviral efficacy. Surface engineering, in particular, plays a key role in enhancing the desired therapeutic effects. However, manipulating the surface characteristics of MXenes can be challenging due to the complexities involved in their synthesis, functionalization, and characterization. In addition, essential properties such as homogeneity, biodegradability, and stability must be thoroughly evaluated for MXenes to be considered suitable for clinical use. Developing cost-effective and environmentally sustainable production methods is vital for the scalable manufacturing of MXene-based materials. Achieving a balance between clinical therapeutic effectiveness and biological safety is crucial for their successful application in healthcare. In conclusion, MXenes hold great promise as an effective solution for combating microbial and viral infections. However, challenges related to toxicity, bio-

 This journal is © The Royal Society of Chemistry 2025

Published on 26 1446. Downloaded on 13/11/47 04:29:14 .

compatibility, and production must be addressed to fully harness their potential. Overcoming these hurdles will enable the successful integration of MXenes into biotechnological and nanomedicine applications.[166]

## 7. Future perspectives and potential applications

The future prospects for MXenes are associated with applications in the biomedical field, including the detection of microbes and viruses, antimicrobial therapy, biosensor development, the production of personal protective equipment, and photocatalytic sterilisation. Furthermore, the combination of MXenes with new composites and hydrogels is anticipated to expand their application in various therapeutic, diagnostic and infection prevention areas. The future application of MXenes is anticipated to extend to a broader range of areas, including cancer therapy, imaging, biosensor development and antimicrobial formulations. However, further research is required to realise this potential in its entirety.

MXenes are a class of two-dimensional transition metal carbides or nitrides that exhibit remarkable properties, including excellent biocompatibility, abundant surface functional groups, high electrical conductivity, and photothermal capabilities. These attributes make them highly promising materials for a range of biomedical applications. MXenes show significant potential in areas such as drug delivery, tissue engineering, antimicrobial treatments, and biosensing, attracting considerable attention in microbiology and virology as well. Due to their high surface area and reactive characteristics, MXenes are particularly well-suited for use in biosensors, especially for pathogen detection. Their ability to interact with environmental changes enables the rapid and sensitive identification of microbes and viruses. MXene-based biosensors are emerging as powerful tools for the early detection of viral infections. Their ability to bind to biomolecules makes them highly effective for quickly identifying viral pathogens, including HIV, Hepatitis, and SARS-CoV-2. Additionally, MXenes possess antimicrobial properties that allow them to inhibit both bacterial and viral growth. These features support the development of antimicrobial surfaces for use in personal protective equipment, such as face masks and medical gowns.[167] The photocatalytic and photothermal properties of MXenes make them ideal candidates for developing advanced photo sterilizers, which can be used in medical devices to eliminate microbial pathogens. Additionally, the integration of cutting-edge manufacturing techniques, such as 3D printing, can enhance the production of personal protective equipment and medical components, allowing for more efficient and precise fabrication.[168] MXenes hold considerable promise for applications in both pathogen detection and antimicrobial therapy, particularly in the fields of microbiology and virology. Within biomedical engineering, MXenes have shown great potential in areas such as regenerative medicine, infection management, cancer treatment, and the development of biosensors. When combined with other materials, MXenes enable the creation of innovative composites and hydrogels. These new materials can be applied in various ways, including the detection, treatment, and prevention of bacterial and viral infections. In the long term, MXenes could play a significant role across multiple biomedical domains, such as cancer therapy, diagnostic imaging, antimicrobial formulations, and biosensor development. However, additional research is needed to fully understand the potential of MXenes in microbiology and virology. Specifically, advancing studies on viral infection detection and treatment could help broaden the use of these materials in medical applications.[169]

## 8. Conclusion

MXenes, with their distinctive properties, hold significant promise in the fields of microbiology and virology. Due to their high surface area and ability to be surface-modified, MXenes enable the rapid and highly sensitive detection of pathogens, positioning them as ideal biosensors for early infection diagnosis. Moreover, their antimicrobial and antiviral activities make them powerful tools in combating antibiotic-resistant infections and viral diseases. Certain MXene variants, in particular, have shown promise in inhibiting bacterial growth and reducing viral replication. MXene-based therapeutic platforms offer innovative solutions for treating microbial and viral infections. These platforms function not only as antimicrobial and antiviral agents but also possess immune-modulatory properties, which could play a key role in infection management and immune response regulation. However, the practical use of MXenes in medical applications faces challenges related to biocompatibility, toxicity, and production scalability. Addressing these issues will be crucial for enabling their widespread clinical adoption. Looking ahead, the potential for MXenes in fighting infections and viruses is vast. These materials have the potential to be central to the development of personalized therapies and more efficient antimicrobial and antiviral systems. Beyond infection treatment, MXenes could contribute to broader biomedical advancements, such as immune modulation and vaccine development. As research progresses, MXenes are poised to become a vital part of future healthcare innovations, influencing both therapeutic strategies and the evolution of treatment modalities.

## Data availability

No primary research results, software or code have been included and no new data were generated or analysed as part of this review.

## Conflicts of interest

There are no conflicts to declare.

Published on 26 1446. Downloaded on 13/11/47 04:29:14 .

## References


1 B. Gürbüz and F. Ciftci, *Chem. Eng. J.*, 2024, **489**, DOI: 10.1016/j.cej.2024.151230.
2 L. Verger, V. Natu, M. Carey and M. W. Barsoum, *Trends Chem.*, 2019, **1**, 656–669, DOI: 10.1016/j.trechm.2019.04.006.
3 X. Lin, *et al.*, *Biomater. Sci.*, 2021, **9**, 5437–5471, DOI: 10.1039/d1bm00526j.
4 S. K. Balu, *et al.*, *J. Environ. Chem. Eng.*, 2022, **10**, 108663, DOI: 10.1016/j.jece.2022.108663.
5 S. Ye, *et al.*, *Front. Bioeng. Biotechnol.*, 2024, **12**, 1338539, DOI: 10.3389/fbioe.2024.1338539.
6 S. Iravani and R. S. Varma, *RSC Adv.*, 2023, **13**, 9665–9677, DOI: 10.1039/d3ra01276j.
7 K. Salimiyan rizi, *J. Mol. Struct.*, 2022, **1262**, 132958, DOI: 10.1016/j.molstruc.2022.132958.
8 M. Alhabeb, *et al.*, *Angew. Chem., Int. Ed.*, 2023, **57**, 5444–5448, DOI: 10.1002/anie.201802232.
9 X. Wang, *et al.*, *J. Mater. Chem. A*, 2017, **5**, 22012–22023, DOI: 10.1039/c7ta01082f.
10 Y. Gogotsi and B. Anasori, *ACS Nano*, 2019, **13**, 8491–8494, DOI: 10.1021/acsnano.9b06394.
11 J. Luo, E. Matios, H. Wang, X. Tao and W. Li, *InfoMat*, 2020, **2**, 1057–1076, DOI: 10.1002/inf2.12118.
12 H. Yu, *et al.*, *Small*, 2019, **15**, 1901503, DOI: 10.1002/smll.201901503.
13 Y. Xu, X. Wang, W. L. Zhang, F. Lv and S. Guo, *Chem. Soc. Rev.*, 2018, **47**, 586–625, DOI: 10.1039/c7cs00500h.
14 B. Shao, *et al.*, *J. Mater. Chem. A*, 2020, **8**, 7508–7535, DOI: 10.1039/d0ta01552k.
15 X. Chen, *et al.*, *Nanoscale*, 2018, **10**, 1111–1118, DOI: 10.1039/c7nr06958h.
16 U. U. Rahman, *et al.*, *Molecules*, 2022, **27**, 4909, DOI: 10.3390/molecules27154909.
17 X. Yu, X. Cai, H. Cui, S. W. Lee, X. F. Yu and B. Liu, *Nanoscale*, 2017, **9**, 17859–17864, DOI: 10.1039/c7nr05997c.
18 J. Chen, H. Cheng, L. X. Ding and H. Wang, *Mater. Chem. Front.*, 2021, **5**, 5954–5969, DOI: 10.1039/d1qm00546d.
19 C. Chiew and M. H. Malakooti, *Mater. Horiz.*, 2023, **10**, 5110–5125, DOI: 10.1039/d3mh00916e.
20 S. V. Lahade, I. Pandey and S. Bhansali, ECS Meeting Abstracts, 2020, MA2020-01, 1880, DOI: 10.1149/ma2020-01271880mtgabs.
21 M. R. Ali, *et al.*, *Crit. Rev. Anal. Chem.*, 2024, **54**, 1381–1398, DOI: 10.1080/10408347.2022.2115286.
22 A. Seitak, *et al.*, *Sens. Actuators Rep.*, 2023, **6**, 100175, DOI: 10.1016/j.snr.2023.100175.
23 Q. Li, *et al.*, *Anal. Methods*, 2021, **13**, 4864–4870, DOI: 10.1039/d1ay00902h.
24 S. Panda, *et al.*, *FlatChem*, 2022, **33**, 100377, DOI: 10.1016/j.flatc.2022.100377.
25 H. Zhang, L. Ma, L. Ma, M. Z. Hua, S. Wang and X. Lu, *Int. J. Food Microbiol.*, 2017, **243**, 64–69, DOI: 10.1016/j.ijfoodmicro.2016.12.003.
26 X. Peng, *et al.*, *Sens. Actuators, B*, 2019, **286**, 222, DOI: 10.1016/j.snb.2019.01.158.
27 G. B. L. Silva, F. V. Campos, M. C. C. Guimarães and J. P. Oliveira, *Pathogens*, 2023, **12**, 1441, DOI: 10.3390/pathogens12121441.
28 R. Bhattacharjee, *et al.*, *OpenNano*, 2022, **8**, 100078, DOI: 10.1016/j.onano.2022.100078.
29 K. R. Chaudhary, S. Kujur and K. Singh, *OpenNano*, 2023, **9**, 100118, DOI: 10.1016/j.onano.2022.100118.
30 C. Liu, D. Xu, X. Dong and Q. Huang, *Trends Food Sci. Technol.*, 2022, **128**, 90–101, DOI: 10.1016/j.tifs.2022.07.012.
31 M. Lin, *Nanotechnology in the Food, Beverage and Nutraceutical Industries*, 2012, pp. 317–334, DOI: 10.1533/9780857095657.2.317.
32 S. Lee, *et al.*, *J. Med. Virol.*, 2023, **95**, 29309, DOI: 10.1002/jmv.29309.
33 A. S. Skof, L. Rotenberg, P. V. F. Hannemann, S. Thies, E. Boschetti-Grützmacher and A. M. Kaufmann, *Diagnostics*, 2023, **13**, 1135, DOI: 10.3390/diagnostics13061135.
34 D. Nidzworski, J. Dobkowska, M. Hołysz, B. Gromadzka and B. Szewczyk, *Cent. Eur. J. Biol.*, 2014, **9**, 628–633, DOI: 10.2478/s11535-014-0296-z.
35 Y. Sun, *et al.*, *Biosens. Bioelectron.*, 2017, **89**, 906–912, DOI: 10.1016/j.bios.2016.09.100.
36 W. Li, *et al.*, *J. Hazard. Mater.*, 2024, **466**, 133019, DOI: 10.1016/j.jhazmat.2023.133019.
37 S. H. Nguyen, V. N. Nguyen and M. T. Tran, *PLoS One*, 2024, **19**, 0297581, DOI: 10.1371/journal.pone.0297581.
38 N. D. Zakaria, H. H. Hamzah, I. L. Salih, V. Balakrishnan and K. Abdul Razak, *Biosensors*, 2023, **13**, 294, DOI: 10.3390/bios13020294.
39 U. O. Kibwana, *et al.*, *Front. Trop. Dis.*, 2024, **5**, 1307379, DOI: 10.3389/fitd.2024.1307379.
40 K. N. Alieva, M. V. Golikova, A. A. Kuznetsova and S. H. Zinner, *Antibiotics*, 2023, **12**, 1170, DOI: 10.3390/antibiotics12071170.
41 Z. Li, *et al.*, *Front. Cell. Infect. Microbiol.*, 2021, **11**, 639473, DOI: 10.3389/fcimb.2021.639473.
42 D. G. Park, *et al.*, *Front. Microbiol.*, 2023, **14**, 1179934, DOI: 10.3389/fmicb.2023.1179934.
43 P. H. Nhung, K. Ohkusu, J. Miyasaka, X. S. Sun and T. Ezaki, *Diagn. Microbiol. Infect. Dis.*, 2007, **59**, 271–275, DOI: 10.1016/j.diagmicrobio.2007.05.016.
44 S. Wang, *et al.*, *Biosens. Bioelectron.*, 2019, **140**, 111333, DOI: 10.1016/j.bios.2019.111333.
45 C. Wiechers, A. L. Bissinger, K. Hamprecht, P. Kimmig, G. Jahn and C. F. Poets, *J. Perinatol.*, 2008, **28**, 79–81, DOI: 10.1038/sj.jp.7211849.
46 Z. Shoja, S. Jalilvand, T. Latifi and F. Roohvand, *Arch. Virol.*, 2022, **167**, 1013–1023, DOI: 10.1007/s00705-022-05407-9.
47 N. Kumar, *et al.*, *PLoS One*, 2016, **11**, 0159027, DOI: 10.1371/journal.pone.0159027.



This journal is © The Royal Society of Chemistry 2025

Published on 26 1446. Downloaded on 13/11/47 04:29:14 .

48 R. A. Halvorson and P. J. Vikesland, *Environ. Sci. Technol.*, 2010, **44**, 7749–7755, DOI: 10.1021/es101228z.
49 G. Martins, *et al.*, *Biosens. Bioelectron.*, 2020, **168**, 112255, DOI: 10.1016/j.bios.2020.112255.
50 D. Pohl, P. M. Keller, V. Bordier and K. Wagner, *World J. Gastroenterol.*, 2019, **25**, 4629–4660, DOI: 10.3748/wjg.v25.i32.4629.
51 S. A. Ahire, A. A. Bachhav, T. B. Pawar, B. S. Jagdale, A. V. Patil and P. B. Koli, *Results Chem.*, 2022, **4**, 100633, DOI: 10.1016/j.rechem.2022.100633.
52 V. Akimov, *et al.*, *Nonequilibrium Carrier Dynamics in Semiconductors*, 2007, vol. 110, pp. 229–232, DOI: 10.1007/978-3-540-36588-4_51.
53 X. F. Chen, X. Zhao and Z. Yang, *Microchim. Acta*, 2022, **189**, 443, DOI: 10.1007/s00604-022-05533-w.
54 N. Reta, C. P. Saint, A. Michelmore, B. Prieto-Simon and N. H. Voelcker, *ACS Appl. Mater. Interfaces*, 2018, **10**, 6055–6072, DOI: 10.1021/acsami.7b13943.
55 Y. Mei, *et al.*, *Food Bioprocess Technol.*, 2022, **15**, 498–513, DOI: 10.1007/s11947-022-02759-7.
56 M. Mohammadniaei, A. Koyappayil, Y. Sun, J. Min and M. H. Lee, *Biosens. Bioelectron.*, 2020, **159**, 112208, DOI: 10.1016/j.bios.2020.112208.
57 S. Wang, *et al.*, *Sens. Actuators, B*, 2023, **380**, 133393, DOI: 10.1016/j.snb.2023.133393.
58 F. Liu, *et al.*, *Anal. Chem.*, 2023, **95**, 14297–14307, DOI: 10.1021/acs.analchem.3c02529.
59 G. Dai, *et al.*, *Food Chem.*, 2023, **424**, 136244, DOI: 10.1016/j.foodchem.2023.136244.
60 S. Ranjbar, N. Ashari Astani, M. Atabay, N. Naseri, A. Esfandiar and M. Reza Ejtehadi, *J. Colloid Interface Sci.*, 2022, **623**, 1063–1074, DOI: 10.1016/j.jcis.2022.05.033.
61 Y. Zheng, *et al.*, *J. Electroanal. Chem.*, 2023, **935**, 117303, DOI: 10.1016/j.jelechem.2023.117303.
62 Y. Li, *et al.*, *ACS Omega*, 2021, **6**, 6643–6653, DOI: 10.1021/acsomega.0c05421.
63 H. Liu, *et al.*, *Talanta*, 2023, **258**, 124433, DOI: 10.1016/j.talanta.2023.124433.
64 Y. Liu, *et al.*, *ACS Appl. Mater. Interfaces*, 2023, **15**, 35872–35883, DOI: 10.1021/acsami.3c05424.
65 R. Chen, *et al.*, *Microchim. Acta*, 2021, **188**, 316, DOI: 10.1007/s00604-021-04974-z.
66 A. Parihar, *et al.*, *Bioelectrochemistry*, 2024, **158**, 108700, DOI: 10.1016/j.bioelechem.2024.108700.
67 S. Lin, *et al.*, *Analyst*, 2021, **146**, 4391–4399, DOI: 10.1039/d1an00606a.
68 Y. Li, *et al.*, *Adv. Mater. Technol.*, 2024, **9**, 2201787, DOI: 10.1002/admt.202201787.
69 W. Y. Chen, H. Lin, A. K. Barui, A. M. U. Gomez, M. K. Wendt and L. A. Stanciu, *ACS Appl. Nano Mater.*, 2022, **5**, 1902–1910, DOI: 10.1021/acsanm.1c03520.
70 A. Ali, *et al.*, *Biosensors*, 2024, **14**, 497, DOI: 10.3390/bios14100497.
71 Y. Wang, *et al.*, *Microchem. J.*, 2021, **167**, 106332, DOI: 10.1016/j.microc.2021.106332.
72 C. Wang, S. Liu and H. Ju, *Bioelectrochemistry*, 2023, **149**, 108281, DOI: 10.1016/j.bioelechem.2022.108281.
73 J. Zhang, Y. Li, S. Duan and F. He, *Anal. Chim. Acta*, 2020, **1123**, 9–17, DOI: 10.1016/j.aca.2020.05.013.
74 L. Wang, K. Cui, P. Wang, M. Pei and W. Guo, *Anal. Bioanal. Chem.*, 2021, **413**, 4353–4362, DOI: 10.1007/s00216-021-03391-8.
75 W. Wei, *et al.*, *Sens. Actuators, B*, 2021, **332**, 129525, DOI: 10.1016/j.snb.2021.129525.
76 X. Jiang, Z. Lv, W. Ding, Y. Zhang and F. Lin, *J. Electrochem. Sci. Technol.*, 2022, **13**, 431–437, DOI: 10.33961/jecst.2022.00269.
77 J. Kochana, A. Pollap and M. Madej, *Handbook of Bioanalytics*, 2022, pp. 729–745, DOI: 10.1007/978-3-030-95660-8_33.
78 M. Kurnik, E. Z. Pang and K. W. Plaxco, *Angew. Chem., Int. Ed.*, 2020, **59**, 8442–18445, DOI: 10.1002/anie.202007256.
79 R. A. Soomro, S. Jawaid, Q. Zhu, Z. Abbas and B. Xu, *Chin. Chem. Lett.*, 2020, **31**, 922–930, DOI: 10.1016/j.cclet.2019.12.005.
80 N. G. Jha, D. S. Dkhar, S. K. Singh, S. J. Malode, N. P. Shetti and P. Chandra, *Biosensors*, 2023, **13**, 235, DOI: 10.3390/bios13020235.
81 L. Li, X. Ji and K. Chen, *J. Biomater. Appl.*, 2023, **37**, 1169–1181, DOI: 10.1177/08853282221131137.
82 D. I. Walker, A. Younger, L. Stockley and C. Baker-Austin, *Food Microbiol.*, 2018, **73**, 29–38, DOI: 10.1016/j.fm.2017.12.006.
83 Y. Mao, X. Huang, S. Xiong, H. Xu, Z. P. Aguilar and Y. Xiong, *Food Control*, 2016, **59**, 601–608, DOI: 10.1016/j.foodcont.2015.06.048.
84 B. Pang, *et al.*, *Anal. Biochem.*, 2018, **542**, 58–62, DOI: 10.1016/j.ab.2017.11.010.
85 X. Ma, J. Li, Y. Liu, Y. Yuan and G. Xu, *Sens. Actuators, B*, 2017, **248**, 201–206, DOI: 10.1016/j.snb.2017.03.172.
86 T. Xu, X. Wang, Y. Huang, K. Lai and Y. Fan, *Food Control*, 2019, **106**, 106720, DOI: 10.1016/j.foodcont.2019.106720.
87 S. L. Drake, A. Depaola and L. A. Jaykus, *Compr. Rev. Food Sci. Food Saf.*, 2007, **6**, 120–144, DOI: 10.1111/j.1541-4337.2007.00022.x.
88 J. Zhang, A. Sheng, P. Wang, J. Yang, L. Tang and F. Chen, *Anal. Chem.*, 2021, **93**, 4676–4681, DOI: 10.1021/acs.analchem.1c00371.
89 Z. Chen, *et al.*, *J. Nanobiotechnol.*, 2023, **21**, 141, DOI: 10.1186/s12951-023-01903-5.
90 H. Niu, *et al.*, *Anal. Methods*, 2022, **14**, 843–849, DOI: 10.1039/d1ay02029c.
91 S. Guenther, D. Huwyler, S. Richard and M. J. Loessner, *Appl. Environ. Microbiol.*, 2009, **75**, 93–100, DOI: 10.1128/AEM.01711-08.
92 S. Shaji, R. K. Selvaraj and R. Shanmugasundaram, *Microorganisms*, 2023, **11**, 2814, DOI: 10.3390/microorganisms11112814.
93 X. Qu, P. Zhou, W. Zhao, B. Shi, Y. Zheng and L. Jiang, *Microchem. J.*, 2024, **199**, 110069, DOI: 10.1016/j.microc.2024.110069.

Published on 26 1446. Downloaded on 13/11/47 04:29:14 .

94 T. Xu, Y. Wang, Y. Xue, J. Li and Y. Wang, *Chem. Eng. J.*, 2023, **470**, 144247, DOI: 10.1016/j.cej.2023.144247.
95 K. Huang, Z. Li, J. Lin, G. Han and P. Huang, *Chem. Soc. Rev.*, 2018, **47**, 5109–5124, DOI: 10.1039/c7cs00838d.
96 R. P. Pandey, K. Rasool, V. E. Madhavan, B. Aïssa, Y. Gogotsi and K. A. Mahmoud, *J. Mater. Chem. A*, 2018, **47**, 5109–5124, DOI: 10.1039/c7ta10888e.
97 F. Ghaemi, *et al.*, *Sustain Cities Soc*, 2021, **72**, 103046, DOI: 10.1016/j.scs.2021.103046.
98 A. Uzunoglu, *et al.*, *Microchem J*, 2023, **193**, 108970, DOI: 10.1016/j.microc.2023.108970.
99 A. Yilmazer, *et al.*, *Small Methods*, 2023, **7**, 2300044, DOI: 10.1002/smtd.202300044.
100 L. Jiang, A. Tang, L. Song, Y. Tong and H. Fan, *Front. Immunol.*, 2023, **14**, 1041149, DOI: 10.3389/fimmu.2023.1041149.
101 J. A. Pulit-Penaloza, *et al.*, *J. Virol.*, 2018, **92**, e00095–e00018, DOI: 10.1128/jvi.00095-18.
102 X. Weng, C. Zhang and H. Jiang, *LWT–Food Sci. Technol.*, 2021, **151**, 112172, DOI: 10.1016/j.lwt.2021.112172.
103 W. Yang, *et al.*, *Biosens. Bioelectron.*, 2023, **235**, 115358, DOI: 10.1016/j.bios.2023.115358.
104 Z. Chen, *et al.*, *J. Nanobiotechnology*, 2023, **21**(1), 141, DOI: 10.1186/s12951-023-01903-5.
105 R. Zeng, *et al.*, *Nano Energy*, 2021, **82**, DOI: 10.1016/j.nanoen.2020.105711.
106 Y. Chen, *et al.*, *J. Colloid Interface Sci.*, 2024, **653**, 540–550, DOI: 10.1016/j.jcis.2023.09.097.
107 N. A. Turner, *et al.*, *Nat. Rev. Microbiol.*, 2019, **17**, 203–218, DOI: 10.1038/s41579-018-0147-4.
108 P. Pino, F. Bosco, C. Mollea and B. Onida, *Pharmaceutics*, 2023, **15**, 970, DOI: 10.3390/pharmaceutics15030970.
109 F. Gao, *et al.*, *Adv. Mater.*, 2023, **35**, 2302559, DOI: 10.1002/adma.202302559.
110 A. Singhwane, K. Chaturvedi, R. K. Mohapatra, A. K. Srivastava and S. Verma, *ACS Symp. Ser.*, 2023, **1443**, 1–17, DOI: 10.1021/bk-2023-1443.ch001.
111 Y. Gao, *et al.*, *J. Colloid Interface Sci.*, 2022, **617**, 533–541, DOI: 10.1016/j.jcis.2022.03.032.
112 F. Seidi, *et al.*, *Small*, 2023, **19**, 2206716, DOI: 10.1002/smll.202206716.
113 W. Hu, *et al.*, *ACS Nano*, 2010, **4**, 4317–4323, DOI: 10.1021/nn101097v.
114 A. Jastrzebska, *et al.*, *Int. J. Electrochem. Sci.*, 2017, **12**, 2159–2172, DOI: 10.20964/2017.03.06.
115 Y. Zhu, *et al.*, *ACS Nano*, 2022, **16**, 3105–3118, DOI: 10.1021/acsnano.1c10732.
116 G. P. Lim, C. F. Soon, M. Morsin, M. K. Ahmad, N. Nayan and K. S. Tee, *Ceram. Int.*, 2020, **46**, 20306–20312, DOI: 10.1016/j.ceramint.2020.05.118.
117 J. Zhu, J. Wang, J. Hou, Y. Zhang, J. Liu and B. Van der Bruggen, *J. Mater. Chem. A*, 2017, **5**, 6776–6793, DOI: 10.1039/c7ta00009j.
118 L. Wang, *et al.*, *Nanoscale*, 2020, **12**, 19516–19535, DOI: 10.1039/d0nr05746k.
119 D. Y. Zhang, *et al.*, *J. Nanobiotechnol.*, 2022, **20**, 53, DOI: 10.1186/s12951-022-01253-8.
120 A. Schön and E. Freire, *Anal. Biochem.*, 2021, **626**, 114240, DOI: 10.1016/j.ab.2021.114240.
121 D. Wu, R. Zhao, Y. Chen, Y. Wang, J. Li and Y. Fan, *Phys. Chem. Chem. Phys.*, 2021, **23**, 3341–3350, DOI: 10.1039/d0cp05928e.
122 S. Roy, S. Sarkhel, D. Bisht, S. N. Hanumantharao, S. Rao and A. Jaiswal, *Biomater. Sci.*, 2022, **10**, 4392–4423, DOI: 10.1039/d2bm00472k.
123 A. M. Amani, *et al.*, *Mater. Today Commun.*, 2024, **41**, 110774, DOI: 10.1016/j.mtcomm.2024.110774.
124 K. Rasool, *et al.*, *Sci. Rep.*, 2017, **7**, 1598, DOI: 10.1038/s41598-017-01714-3.
125 H. Lin, S. Gao, C. Dai, Y. Chen and J. Shi, *J. Am. Chem. Soc.*, 2017, **139**, 16235–16247, DOI: 10.1021/jacs.7b07818.
126 Z. O. Uygun and S. Tasoglu, *iScience*, 2024, **27**, 109190, DOI: 10.1016/j.isci.2024.109190.
127 K. Chaturvedi, *et al.*, *Top. Curr. Chem.*, 2023, **381**, 11, DOI: 10.1007/s41061-023-00420-1.
128 F. Alimohammadi, *et al.*, *Langmuir*, 2018, **34**, 7192–7200, DOI: 10.1021/acs.langmuir.8b00262.
129 K. Rasool, *et al.*, *ACS Nano*, 2016, **10**, 3674–3684, DOI: 10.1021/acsnano.6b00181.
130 R. P. Pandey, *et al.*, *ACS Appl. Nano Mater.*, 2020, **3**, 11372–11382, DOI: 10.1021/acsanm.0c02463.
131 A. Shamsabadi, *et al.*, *ACS Sustainable Chem. Eng.*, 2018, **6**, 16586–16596, DOI: 10.1021/acssuschemeng.8b03823.
132 A. M. Jastrzębska, *et al.*, *Mater. Sci. Eng., C*, 2021, **119**, 111431, DOI: 10.1016/j.msec.2020.111431.
133 K. Zheng, *et al.*, *Adv. Healthcare Mater.*, 2020, **9**(19), e2001007, DOI: 10.1002/adhm.202001007.
134 B. Ezraty, A. Gennaris, F. Barras and J. F. Collet, *Nat. Rev. Microbiol.*, 2017, **15**, 385–396, DOI: 10.1038/nrmicro.2017.26.
135 Q. Zou, M. Abbas, L. Zhao, S. Li, G. Shen and X. Yan, *J. Am. Chem. Soc.*, 2017, **139**, 1921–1927, DOI: 10.1021/jacs.6b11382.
136 F. Wu, *et al.*, *Sci. China Mater.*, 2020, **1–11**, 748, DOI: 10.1007/s40843-020-1451-7.
137 X. Cheng, X. Qin, Z. Su, X. Gou, Z. Yang and H. Wang, *Nanomaterials*, 2023, **13**, 2121, DOI: 10.3390/nano13142121.
138 M. S. Salmi, U. Ahmed, N. Aslfattahi, S. Rahman, J. G. Hardy and A. Anwar, *RSC Adv.*, 2022, **12**, 33142–33155, DOI: 10.1039/d2ra04944a.
139 Z. Shi, *et al.*, *Sens. Actuators, B*, 2023, **383**, 133598, DOI: 10.1016/j.snb.2023.133598.
140 C. Bhandari, *et al.*, *Nano Today*, 2021, **36**, 101052, DOI: 10.1016/j.nantod.2020.101052.
141 A. Rosenkranz, *et al.*, *Appl. Surf. Sci.*, 2021, **567**, 150795, DOI: 10.1016/j.apsusc.2021.150795.
142 M. A. Unal, *et al.*, *Nano Today*, 2021, **38**, 101136, DOI: 10.1016/j.nantod.2021.101136.


This journal is © The Royal Society of Chemistry 2025

Published on 26 1446. Downloaded on 13/11/47 04:29:14 .

143 E. Ghasemy, A. Miri Jahromi, M. Khedri, P. Zandi, R. Maleki and L. Tayebi, *J. Biomol. Struct. Dyn.*, 2022, **40**, 11460–11466, DOI: **10.1080/07391102.2021.1957711**.
144 M. Khatami, P. Iravani, G. Jamalipour Soufi and S. Iravani, *Mater. Technol.*, 2022, **37**, 1890–1905, DOI: **10.1080/10667857.2021.2002587**.
145 T. Tong, W. Tang, S. Xiao and J. Liang, *Adv. NanoBiomed Res.*, 2022, **2**, 2200067, DOI: **10.1002/anbr.202200067**.
146 Y. Hu, *et al.*, *Talanta*, 2024, **125101**, 266, DOI: **10.1016/j.talanta.2023.125101**.
147 W. J. Zhang, *et al.*, *Int. J. Mol. Sci.*, 2022, **23**, 14925, DOI: **10.3390/ijms232314925**.
148 C. Yang, Y. Luo, H. Lin, M. Ge, J. Shi and X. Zhang, *ACS Nano*, 2021, **15**, 1086–1099, DOI: **10.1021/acsnano.0c08045**.
149 S. Zhang, *et al.*, *J. Colloid Interface Sci.*, 2021, **599**, 390–403, DOI: **10.1016/j.jcis.2021.04.109**.
150 Y. Fu, *et al.*, *Appl. Surf. Sci.*, 2022, **598**, 153783, DOI: **10.1016/j.apsusc.2022.153783**.
151 M. Liu, *et al.*, *Front. Bioeng. Biotechnol.*, 2023, **11**, 1308184, DOI: **10.3389/fbioe.2023.1308184**.
152 M. Mansoorianfar, K. Shahin, A. Hojjati-Najafabadi and R. Pei, *Chemosphere*, 2022, **290**, 133383, DOI: **10.1016/j.chemosphere.2021.133383**.
153 M. Koohkhezri, *et al.*, *ACS Applied Bio Materials*, 2024, **11**, 7244–7255, DOI: **10.1021/acsabm.4c00880**.
154 X. Li, *et al.*, *Adv. Mater. Technol.*, 2022, **7**, 2100872, DOI: **10.1002/admt.202100872**.
155 C. Yu, *et al.*, *Colloids Surf., B*, 2022, **217**, 112663, DOI: **10.1016/j.colsurfb.2022.112663**.
156 Q. Wu, *et al.*, *Appl. Catal., B*, 2021, **297**, 120500, DOI: **10.1016/j.apcatb.2021.120500**.
157 Y. Liu, *et al.*, *Chem. Eng. J.*, 2021, **410**, 128209, DOI: **10.1016/j.cej.2020.128209**.
158 Y. Zheng, *et al.*, *Acta Biomater.*, 2022, **410**, 128209, DOI: **10.1016/j.actbio.2022.02.019**.
159 N. Ding, *et al.*, *ACS Appl. Mater. Interfaces*, 2024, DOI: **10.1021/acsami.4c03587**.
160 W. Zhao, *et al.*, *Appl. Phys. A*, 2023, **129**, DOI: **10.1007/s00339-023-06602-4**.
161 I. H. Naser, *Chem. Biodiversity*, 2024, DOI: **10.1002/cbdv.202400366**.
162 F. Liu, *et al.*, *ACS Appl. Mater. Interfaces*, 2024, **16**, 10148–10157, DOI: **10.1021/acsami.3c18227**.
163 N. Kwon, S. Lee, M. Jang, J. H. Lee, C. Park and T. Lee, *Biochip J.*, 2024, **18**, 93–102, DOI: **10.1007/s13206-023-00133-z**.
164 S. Iravani and R. S. Varma, *Chem. Commun.*, 2022, **58**, 7336–7350, DOI: **10.1039/d2cc01694j**.
165 A. Szuplewska, *et al.*, *Trends Biotechnol.*, 2020, **38**, 264–279, DOI: **10.1016/j.tibtech.2019.09.001**.
166 S. Iravani and R. S. Varma, *Mater. Adv.*, 2021, **2**, 2906–2917, DOI: **10.1039/d1ma00189b**.
167 I. C. Lee, *et al.*, *Mater. Horiz.*, 2023, **11**, 876–902, DOI: **10.1039/d3mh01588b**.
168 N. Dwivedi, C. Dhand, P. Kumar and A. K. Srivastava, *Mater. Adv.*, 2021, **2**, 2892–2905, DOI: **10.1039/d1ma00003a**.
169 A. Maleki, *et al.*, *Adv. Funct. Mater.*, 2022, **32**, 34, DOI: **10.1002/adfm.202203430**.